Future Batteries 10 (2026) 100176

Contents lists available at ScienceDirect

Future Batteries

journal homepage: www.sciencedirect.com/journal/future-batteries

Ultrasound-induced delamination of solvent-based lithium-ion battery cathodes for direct recycling: Investigating process parameters and green solvent alternatives ☆

Steffen Kaiser [a,*], Christian Geier [a], Alexander Kessler [a], Christoforos Zamparas [b], Elisabeth Eiche [b], Marco Gleiß [a]

[a] Institute of Mechanical Process Engineering and Mechanics, Karlsruhe Institute of Technology, Straße am Forum 8, Karlsruhe, 76131, Germany
[b] Institute of Applied Geosciences, Karlsruhe Institute of Technology, Karlsruhe, 76131, Germany

ARTICLE INFO

Keywords:
Lithium-ion battery direct recycling
Industrial production scrap
Ultrasound delamination process parameters
Metal impurities
Green solvents

ABSTRACT

Ultrasound is a commonly used tool to aid cleaning of microscopic or soluble contamination. Transferred to battery electrodes, it can be applied to remove active material and binder from the current collector foil. Many direct recycling studies make use of it as an effective delamination method, but rarely investigate in the process parameters. This work considers frequency, temperature, residence time and type of solvent as important adjusting screws to gain a valuable recycling product.

Triethyl phosphate as a non-critical solvent alternative reached fast and similarly good delamination results to the common N-methyl-2-pyrrolidone close to 100 %, while dimethyl sulfoxide caused undesirable structural changes of the lithium-nickel-manganese-cobalt-oxide cathode active material observed by X-ray diffractometry. Others like cyrene, ethyl acetoacetate and acetone did not reach sufficient delamination degree, which was below 31 %. In general, elevated temperatures were necessary to enable dissolution of the binder, but no significant difference between 60 °C and 80 °C was observed.

29 kHz ultrasound frequency generates strong cavitation micro jets, which delaminated the electrode efficiently. It reached a delamination degree of (101.4 ± 0.6) %, but also caused plenty pitting of the current collector foil. This resulted in 4478 ppm of additional aluminum in the inductively coupled plasma optical emission spectroscopy of the recyclate and would make battery manufacturers reject the material. A frequency of 120 kHz reached complete delamination ((100.5 ± 0.3) %) without pitting and exceeded the initial aluminum content by just 121 ppm. The cavitation micro jets at higher frequencies are of greater number concentration, but less energetic, and spare the foil from pitting with simultaneously high delamination degree.

In literature, ultrasound treatment has been described as a promising way to regain active material during direct battery recycling. This study carries on these investigations and gives further insights in the process step. It demonstrates the importance of the process parameters, especially the so far often neglected frequency, and the solvent phase, for a successful recycling.

Introduction

The Joint Research Center of the European Commission predicts a multiplication of the material demand for LIBs due to the upcoming energy transition [1]. The massive need for these materials leads to social, political and environmental issues [2,3]. The recycling of battery materials is essential to set up a circular economy and helps to reduce the need for mining and the import of critical materials [4]. End-of-life (EoL)-batteries as well as production scrap are subject to research in battery recycling. While EoL-batteries impact recycling capacities delayed by their lifetime, production scrap accrues immediately during manufacturing. According to the Battery 2030 report of McKinsey and the Global Battery Alliance [5], about 600 kt a^{-1} of production scrap are expected in 2030. It can be categorized in dry and wet scrap, depending on whether they have become into contact with electrolyte or not. Dry scrap consists of defective coatings e.g. from start-up or shut down, stamping residues and defective electrode stacks or non-filled cells. Wet production scrap originates from electrolyte-filled and formed cells which do not meet the quality requirements. In contrast

☆ This article is part of a Special issue entitled: 'Manufacturing & Recycling' published in Future Batteries.

* Corresponding author.
E-mail address: steffen.kaiser@kit.edu (S. Kaiser).

https://doi.org/10.1016/j.fub.2026.100176
Received 9 February 2026; Received in revised form 20 March 2026; Accepted 3 April 2026
Available online 24 April 2026

Symbol		Unit/Dimension
c	speed of sound	$m\,s^{-1}$
D	degree of delamination	–
d	diameter	m
f	frequency	s^{-1}
g	gravity	$m\,s^{-2}$
h	height	m
i	integer coefficient, number	–
L_{CN}	cavitation noise level	–
m	mass	kg
n	rotation speed	s^{-1}
$\mathbb{N}$	natural numbers	–
Q_{int}	intensity-weighed distribution	–
R	radius in Hansen space	$kg^{0.5}m^{-0.5}s^{-1}$
RCF	relative centrifugal force	–
T	temperature	K
t	time	s
v	velocity	$m\,s^{-1}$
V	volume	m^3
x	particle size, diameter	m
β	mass concentration	$kg\,m^{-3}$
δ	Hansen parameters	$kg^{0.5}m^{-0.5}s^{-1}$
η	dynamic viscosity	$kg\,m^{-1}\,s^{-1}$
θ	scattering angle	°
ϑ	temperature	°C
λ	wavelength	m
ρ	density	$kg\,m^{-3}$
ω	mass fraction	–

to wet production scrap and EoL-batteries, the active material in dry scrap is not degraded from formation or battery usage, nor mixed with different battery types. This makes it a valuable resource to recycling.

Paths of recycling

The pyro- and hydrometallurgical recycling processes are established on industrial scale [6–10] and are mainly designed to regain the high-value metallic components from EoL-batteries, leaving others non-targeted. Pyrometallurgical recycling involves the high-temperature smelting of spent LIBs, while hydrometallurgical recycling uses aqueous solutions to leach metals from cathode materials [4,11–13]. In case of recycling EoL-LIBs, the degraded materials need to be renewed, so the break down to the level of elements during pyro- and hydrometallurgical paths seem reasonable. Pristine active material can then be resnythesized from the recycling products.

Recycling non-degraded dry production scrap through pyro- or hydromatallurgical processes means to destroy the intact chemical and crystallographic structure of the active material. It needs to be expensively resynthesized from its precursors. Direct recycling methods address this drawback. Instead of regaining the constitute elements from the LIBs, recovery takes place on the particle level, preserving the material's structure. The substantial effort invested in producing active materials along the value chain is obtained due to the higher value level of the recyclate. Owing to the greater economic efficiency as well as the simple set-up, the method is especially interesting to battery manufacturers running an in-house recycling for their residues. [4,14–18]

The main task in direct recycling of dry production scrap is the delamination of the current collector and the contamination-free recovery of the active material. [14,17,19–21] If the electrodes have not yet been assembled or degraded, neither a complex separation as pretreatment, nor a regeneration of the spent material as post-treatment is needed. The delaminated active material can directly be reused in the production. In case of readily assembled cells, a disassembly needs to be installed upstream.

Crushing and sieving, thermal decomposition or solvent dissolution of the binder are commonly used to free/release the active material particles from the electrode foil. However, each of the methods faces its own challenges. But still, direct recycling of production scrap can be a worthwhile process. Several publications therefore deal with the upcoming challenges: Crushing is associated with particulate copper and aluminum contamination of the recyclate [14,19,22,23], while thermal decomposition consumes a lot of energy and might release aggressive fluorine components [24–30]. The dissolution of the binder can be time-consuming and implies the application of a solvent [14,28,31,32]. Also other alternative methods for delamination like mechanical brushing or ultrasonication are investigated to efficiently delaminate the production scrap for its direct recycling [28,33–36].

Solvents and ultrasound in LIB recycling

In LIB-anodes, the water-based binder system of styrene-butadiene-rubber and carboxymethyl cellulose replaced the PVDF with NMP in favor of safety and costs [37]. This simplifies the production as well as the recycling of LIB-anodes. Wiechers et al. [34] developed a simple and efficient recycling path for anode scrap assisting the binder dissolution in water by ultrasonication. In extension to Wiechers et al. [34] and Ren et al. [38], this study deals with the challenges of strong adhesive forces by the PVDF-binder in the cathode.

In LIB-cathodes, PVDF is the predominant binder which brings up some challenges. Main problem is the requirement for an aprotic-polar solvent. The most commonly used solvent to dissolve PVDF is the reproductive toxic solvent NMP [39], which has been added to the Registration, Evaluation and Authorization of Chemicals (REACH) list [40]. This is an issue for safety at work and environmental concerns, which has been addressed in context of LIB-production as well as of recycling. Several less problematic, sustainable and green alternative solvents like TEP, DMSO, GVLA, dimethyl isosorbide (DMI) etc. have been assessed to substitute NMP. However, the dissolving properties for PVDF of all of them are poorer than NMP. [30,31,41–47] Therefore simple stirring induced delamination of the cathode can be inefficient: Taking a long time, consuming a lot of solvent, requiring elevated temperatures or other energy inputs. Ultrasonication can be an option to highly improve the dissolution of polymeric PVDF binder in an organic solvent. It assists the dissolution process, as well as the mechanical removal of the coating by cavitation. This seems to be a promising approach to perform the delamination applying solvent alternatives in an effective manner. [35,36,42,48,49]

Idea of this study

In the present study, a combination of ultrasound assistance and the optimization of process parameters enables the application of green solvent alternatives with high delamination degree, despite their partially worse dissolution properties.

- *Green solvent alternatives:* Designing a recycling process is guided by the principles of environmental, economic, and social sustainability. However, the use of NMP contradicts these sustainability goals, making it desirable to replace this hazardous solvent. Green solvent alternatives are therefore made an objective of this study, even though they introduce certain challenges: In former studies they did not reach as high delamination degree as NMP or required elevated process parameters [31,48]. Ahuis et al. [31] performed a solvent-based recovery of shredded cathode scrap in a stirred vessel. They reached recovery yields close to 70 % using NMP at room temperature or TEP at 75 °C as solvents. He et al. [48] reached 99 % of delamination in NMP using an ultrasonic bath at 40 kHz. The idea of applying solvent alternatives has been introduced, but was not pursued under optimized

parameters, as their delamination was less effective in the beginning. Conversely, the effect of temperature, power and time was investigated on NMP, which was taken up for the green solvents in this study.

- *Fast and high delamination degree:* In terms of industrial applicability, close to complete delamination is necessary and should be reached within reasonable time. It is reported that ultrasonication can accelerate the solvent-based binder dissolution [36,38]. Hence, an ultrasound based process was chosen for this study.

Metal impurities play a crucial role in terms of reusability of the recyclate. Even if batteries are running with higher metal content, manufacturers demands are usually strict. Goal of this study is to provide a high-quality recycling product with little impurities by optimizing the ultrasound process parameters.

- *Analysis of metal impurities:* Lei et al. [35] applied high power ultrasonication with 2200 W and 70 W cm^{-2} at 20 kHz to delaminate spent LIB-cathodes. They swiftly reached up to 99.5 % of delamination. Despite the observation of pitting, the contamination of the recyclate has not been investigated, although crucial for the reuse case. He et al. [48] reported an aluminum content of 0.08 wt %. This value shall be undercut to generate a more pure and high-value recycling product. This study provides an analysis of contamination due to pitting of the current collector foil caused by ultrasound cavitation as a base to optimize the process parameters.
- *Ultrasound process parameters:* Some studies [31,42,48,50] investigated the impact of temperature, power and time. Anyway, there is little research considering ultrasound frequency as an important parameter for the delamination step, although it is of high relevance for impurity generation [51]. All of the mentioned parameters are of high significance because they can influence the degree of delamination, the mechanical integrity of the active material as well as the level of contamination. Therefore, this study takes all of them into account to develop a sustainable and cost-saving direct recycling approach for solvent-based LIB-cathode production scrap.

Ultrasound treatment and green solvent alternatives can enhance the mechanical direct recycling. This work combines both and presents a simple and efficient recycling process for solvent-based LIB-cathode production scrap. All dry residues that have not yet come into contact with electrolytes can be recycled without any pre-treatment. This can include defective coatings before and after calendaring or punching residues. In future, the process will be extended for wet rejects and EoL-LIBs which necessitates a disassembly and drying step. Those are also part of the research project this study belongs to and are investigated by Henschel et al. [52] and Lödige et al. [53].

The active material coated current collector foils are inserted into a suitable solvent and are exposed to an ultrasound cleaning device for delamination. Green solvent alternatives were applied as process liquids. Process parameters like temperature, residence time and ultrasound frequency are varied and evaluated in terms of delamination degree and the recycling material's quality. The delamination step results in a diluted suspension of active material and its additives. It can be rethickened for producing 100 % recycling electrodes [34] or added to the manufacturing process [31].

Materials and methods

Raw materials

Goal of this study is to develop an optimized ultrasound assisted recycling process which is suitable for industrial cathodes. Cathode production scrap was hence sourced from a gigafactory for automotive batteries. It has been produced from nickel rich NMC cathode active material (CAM) with a stoichiometry of > 811, carbon based conductive additive (CA) and from PVDF as polymeric binder. NMP was used as solvent to prepare the slurry. The current collector is a 13 µm thick aluminum foil. The coating was double-sided and has been calendared. As a label for this material, indCath is established throughout this work. The composition is given in Table 1. The pristine NMC powder has been supplied for the purpose of analysis too. Both are stored in an argon-filled glovebox (PureSmart T3, Jacomex, France) at <10 ppm H_2O.

Table 1
Composition of the cathode production scrap used as source material: industrial cathode (indCath), laboratory cathode (labCath).

Compound	Unit	indCath	labCath
NMC	wt %	>95.0	94.0
CA	wt %	<2.5	3.0
PVDF	wt %	<2.5	3.0
Solvent	–	NMP	TEP
Solid content	wt %	unknown	67
Foil	µm	13	16
Load	g m^{-2}	165	178
Coating	–	double-sided	single-sided

Self-produced cathodes are used in parallel during this study. According to Chen et al. [45], TEP can be equally used to substitute NMP as a solvent in battery production. This is applied here in favor of safety and environment. At first 0.67 g of PVDF-binder (HSV9300, Gelon LIB Group, China | MSE12201S-000-D0, Sartorius, Germany) were dissolved in 102.31 mL TEP (Triethyl phosphate 99%, Acros Organics, Belgium | Blaubrand Eterna, Brand, Germany) for 4 h at 65 °C in a wide neck bottle (Rasotherm laboratory bottles borosilicate glass, 3.3 Scherf-Präzision, Germany) on a magnetic stirrer (RCT basic, IKA, Germany). The following mixing of the slurry with CA and CAM takes place in the glovebox. 6.67 g of carbon black (CB) (C-NERGY Super C65, Imerys, France) and 208.92 g of NMC811 (S85E, Gelon LIB Group, China) were prepared on a weighing dish (LC6201S, Sartorius, Germany). First, an overhead mixer (Eurostar 60 control, IKA, Germany) with a dissolver stirring tool predispersed the CB for 30 min at 1200 min^{-1} in the PVDF-TEP-solution. NMC was stirred in at the same speed for 2 h afterwards. To prevent the slurry from segregation, it is coated onto the aluminum foil (16 µm · 280 mm Al-foil roll, Gelon LIB Group, China) immediately using a doctor blade with a height of 120 µm (BEVS1818 mini film applicator & BEVS18063/150, BEVS, China). The two-stage drying process is similar to Chen et al. [45]. It starts in an oven (UN110, Memmert, Germany) at 60 °C for at least 6 h and ends in an vacuum oven (RVT360, Heraeus, Germany) at 120 °C after another 6 h. The readily prepared in-house cathodes are subsequently stored in the glovebox again. labCath is the label to distinguish them from the industrial ones. In preparation for the experiments, coin-like plates were punched out of the cathodes.

Acknowledge that materials and chemicals used in this study may cause serious health problems. It is essential to consult safety data sheets of your supplier and to set up a safe working procedure if you try to reproduce this experiments.

Choice of solvent alternatives

The main demand to a solvent in cathode production, as well as in this direct recycling process, is to easily dissolve the PVDF-binder. Hansen et al. [54] developed a method to predict if a material (typically a polymer) will dissolve in a solvent. It is found on the concept that like dissolves like, which means the intermolecular interactions of material and solvent are alike. Each molecule is therefore characterized by three Hansen parameters for dispersion forces δ_d, dipolar forces δ_p and hydrogen bonds δ_h. If the distance between a polymer (index 1) and a solvent (index 2) in Hansen space R_a calculated by Eq. (1) is less than the so called interaction radius R_o, the solid will probably dissolve [54].

$$R_a = \sqrt{4(\delta_{d2} - \delta_{d1})^2 + (\delta_{p2} - \delta_{p1})^2 + (\delta_{h2} - \delta_{h1})^2} \quad (1)$$

Table 2
Selection of possible polyvinylidene fluoride (PVDF) dissolving solvents according to Hansen et al. [54] and Bottino et al. [57] for lithium-ion battery cathode production and recycling and their Hansen solubility parameters δ including the distance in Hansen space R_a and their evaporation temperature and their globally harmonized system of classification and labelling of chemicals (GHS)-symbols [58].

Molecule	δ_d/MPa$^{0.5}$	δ_p/MPa$^{0.5}$	δ_h/MPa$^{0.5}$	R_a/MPa$^{0.5}$	ϑ_v/°C	GHS-symbols
Polyvinylidene fluoride	17.20	12.50	9.20			
N-methyl-2-pyrrolidone	18.00	12.30	7.20	2.57	203	
Triethyl phosphate	16.80	11.50	9.20	1.28	215	
Ethyl acetoacetate	16.50	10.80	8.30	2.38	180	none
γ-valerolactone	18.50	14.10	6.60	4.01	207	none
Cyrene	18.80	10.60	6.90	4.37	227	
Acetone	15.50	10.40	7.00	4.56	56	
Dimethyl sulfoxide	18.40	16.40	10.20	4.69	189	none

The possible solvents have now been chosen by minimizing R_a and rejecting highly hazardous, poorly available or expensive chemicals. This study focuses on TEP as its R_a to PVDF of 1.28 MPa$^{0.5}$ is the smallest among the remaining aprotic-polar solvents and it was successfully tested for battery production [43,45]. Further biorenewable NMP alternatives like Cyrene [44], γ-valerolactone [55] and DMSO [43] have been investigated for LIB-manufacturing and were additionally included in the solvent selection. Data on the process compatibility of these solvents can be found in literature [45,55,56]. Acetone as a common solvent and EAA with promising Hansen parameters were considered in this study too. Table 2 lists the chosen solvents and their Hansen solubility parameters including the distance to PVDF in Hansen space.

The solvents have been sourced from the following suppliers: NMP (Superclo Emplura 1-Methyl-2-pyrrolidone, Merck, Germany), TEP (Triethyl phosphate 99%, Acros Organics), EAA (Ethyl acetoacetate for analysis, Merck, Germany), GVLA (γ-valerolactone 98%, ThermoFisher, Germany), cyrene (Cyrene 99%, Merck, Germany), acetone (Aceton rein, Hugo Häffner Vertrieb, Germany) and DMSO (Dimethyl sulfoxide < 0.03% water for analysis, VWR, France).

Experimental set-up

This study consists of two experimental procedures: Firstly, the parameters for decoating were studied using single plates of indCath on a 10 mL-scale. Secondly, the best parameter setting was chosen and investigated under increasing solid content. This was additionally performed using labCath highlighted by purple color in Fig. 1. In contrast to indCath, the labCath do not underlie non-disclosure restrictions for analytical methods. All the experiments were run in triplicates to proof reproducibility and to give a standard deviation.

Delamination parameters

In the light of future scale-up, two commercially available ultrasound resonators by Weber Ultrasonics were chosen. They are usually applied in bigger industrial context e.g. cleaning of metal components or textiles and can simply be scaled-up [59]. One of them is a multi-frequency resonator (PSW200 W 40-80-120kHz + MG200 TFDMF 40-80-120, Weber Ultrasonics, Germany), which is able to operate at different frequencies: 40 kHz, 80 kHz and 120 kHz. The second (PSW200 W 25 kHz + ULC premium 29 kHz, Weber Ultrasonics, Germany) is solely for 29 kHz. Pre-experiments showed that an operation at 80 kHz is far worse than the other frequencies. It reached its maximal degree of delamination (16.0 ± 6.2) % at 60 °C, with 10 mL of solvent after 15 min. A central reason might be the lowest cavitation activity among the other frequencies at constant generator power, indicated by the cavitation noise level given in Table 3. 80 kHz was therefore not further considered. Anyway, the power of the ultrasound generator was chosen as comparative parameter over cavitation activity because energy consumption of the process is decisive for future industrial applications. It is furthermore not possible to adjust the nominal power of the generator, and power regulation by pulse-width modulation would introduce an additional disparity. The ultrasound generators were run in their standard mode, which means 200 W continuous ultrasonication without pulse-width modulation, but with sweeping function and amplitude modulation. These options are used to improve the cleaning efficiency and also enhance the delamination of electrodes like Yamada et al. [51] showed.

Table 3
Cavitation noise in the ultrasonic bath measured according to IEC TS 63001:2019 Ed.1 with Kavimeter, Elma Schmidbauer, Germany.

Frequency	f/kHz	29	40	80	120
Cavitation noise	L_{CN}/dB	36.80	35.80	27.87	28.63

The 200 W ultrasound resonator is mounted at the bottom of a ~5 L stainless steel basin, which is water-filled. A convector heater (ED, Julabo, Germany) circulated and tempered the water to the desired temperature (Qtemp 200, VWR, Germany) of 60 °C and 80 °C. Experiments without heating were not included, because pre-experiments, as well as Chen et al. [45], did not give reason to expect the PVDF-binder to dissolve in TEP at room temperature. 10 mL (Research Plus, Eppendorf, Germany) of solvent was poured over a plate of indCath in a 100 mL-laboratory bottle (Rasotherm laboratory bottles borosilicate glass, 3.3 Scherf-Präzision, Germany). A stainless steel basket constantly defined the position of the sample. It was placed in the middle of the smaller sub-units, the ultrasonic resonator is made of.

The belly of the standing ultrasound wave in the basin should ideally define the height of the basket to reach the best exposure of the sample. It is located at a multiple integer $i \in \mathbb{N}$ of half the wavelength $\lambda/2$ from the resonator [60]. Several different phases between the resonator and the sample (water, glass, solvent), as well as the frequency sweep function, complicate the prediction of an optimal distance massively. It was therefore determined experimentally: h(29 kHz) = 32 mm and h(40 kHz, 80 kHz and 120 kHz) = 27 mm. The slight effect of temperature on the speed of sound and wavelength $dc/dT = 2.5\,\mathrm{m\,s^{-1}\,K^{-1}}$ [60] can be neglected.

The bottle was removed from the ultrasound bath after a defined time. To investigate the effect of residence time, the experiments were repeated with different settings between 1 min and 15 min. The remaining plate was picked out of the bottle, gently rinsed, dried in a weighing dish at 60 °C over night and used to calculate the delamination degree D. The generated suspension, containing the target CAM, was subject to analysis described in Section "Analytical methods". The degree of delamination D gives a value for the fraction of cathode coating which has been removed from the current collector foil. The initial mass of the plate m_{plate}, the mass after decoating m_{decoat} and a mean mass of the aluminum foil m_{Al} underneath the coating is weighed (PBA224I-1S-FC, VWR, Germany) to calculate D according to Eq. (2).

$$D = \frac{m_{plate} - m_{decoat}}{m_{plate} - m_{Al}} \tag{2}$$

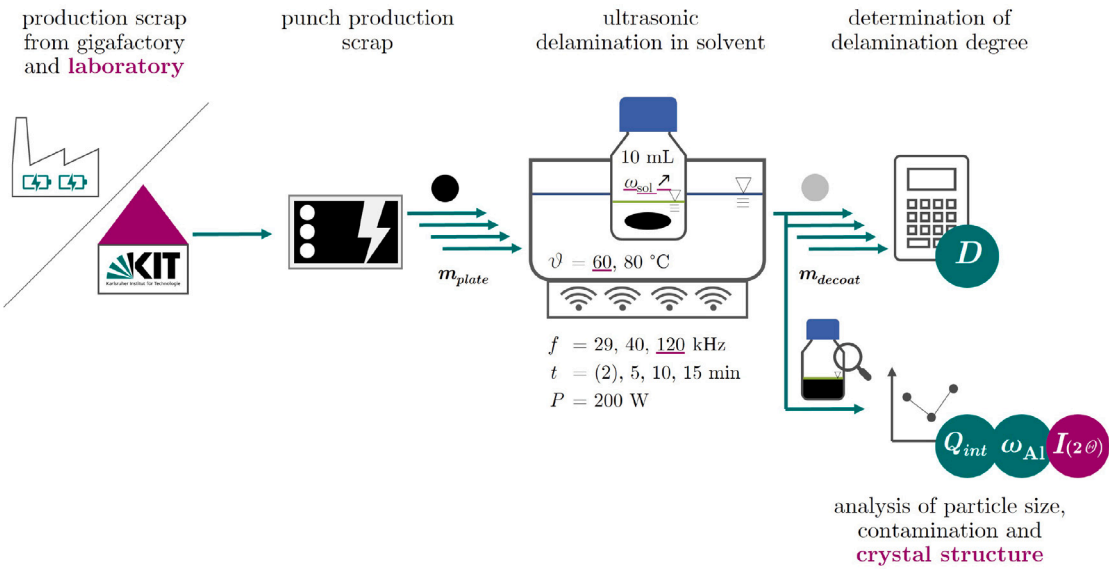

Fig. 1. Schematic experimental procedure to determine the ultrasonic delamination degree of industrial cathode production scrap and the properties of the recycling suspension on 10 mL-scale (green) and of laboratory cathodes with additional crystallographic material analysis (purple).

The best parameters using TEP were repeated with the solvents mentioned in Section "Choice of solvent alternatives" to provide a variety of possible green process liquids for direct LIB-cathode recycling. An experiment with NMP serves as benchmark to compare the results of the green substituents.

To sum up, the parameters temperature, frequency, time and solvent were investigated while keeping the ultrasound power and liquid volume constant.

Increasing solid content

It is intended to use as less volume of solvent as possible in order to save costs and energy for the solvent and the following separation steps. This corresponds with a preferably high solid content in the recycling suspension after the delamination step. An adjusted experimental procedure was derived from Section "Delamination parameters": Several cathode plates were consecutively delaminated in the same bottle with 10 mL of TEP. As a result, the solid content of the recycling suspension was increased step by step. This is indicated by the multiple arrows in Fig. 1. The experiment was performed using indCath, shown in green, as well as labCath, shown in purple.

Analytical methods

Particle size distribution (PSD)

The particle size of the CAM is intentional engineered to adjust the LIB's properties. It should be obtained during the recycling process to possibly reuse the material over and over. PSD is mean of choice to assess the mechanical integrity of the particles. It was determined for the pristine materials, as well as the recycling suspension, based on their sedimentation behavior in a liquid phase. The sample is centrifuged in an analytical centrifuge (LUMiSizer, LUM, Germany) while simultaneously recording the transmission profile of monochromatic light (λ = 870 nm) along the cuvette height. The SEP-View software then calculates the sedimentation velocity distribution of the particles from the change of transmission profiles after predefined time intervals. According to Stoke's Eq. (3) (modified from [61]), the parameters particle density ρ_p, fluid density ρ_f, the viscosity η and the relative centrifugal force RCF are needed to convert the sedimentation velocity v to an equivalent particle diameter x_{eq}. The density and viscosity are parameters given by the substances, while RCF results from the selectable centrifugal speed and the radius. Outcome of this analysis is a cumulative intensity distribution Q_{int} of the sedimentation-velocity-equivalent particle diameter x_{eq}. Further insights in this method are given by Lerche et al. [62].

$$x_{eq} = \sqrt{\frac{18 \cdot \eta \cdot v}{(\rho_p - \rho_f) \cdot RCF \cdot g}} \tag{3}$$

For reliable results some requirements must be fulfilled: The sample needs to be lightly translucent to show a measurable change of its transmission profile from the very beginning of the analysis. Otherwise the bigger particle size fractions will not be detected. On the other hand, the particle concentration should be high enough not to impair the resolution of the PSD. An initial transmission of around 20 % was found to be suitable by Yildiz et al. [63] who validated this method for aqueous anode slurries. In case of this study, it was reached by adjusting the sample concentration to around 3 g L^{-1} with additional solvent. A serial dilution yielded comparable results between 1.2 g L^{-1} and 4.7 g L^{-1}. Measurements of artificially generated recycling suspensions with different PVDF-content did not indicate an impact of the binder on the PSD in this range of concentration.

During the sedimentation analysis, the bigger and denser NMC-particles will sink much faster than the smaller and lighter CB-particles. The standard operating procedure of the LUMiSizer is consequently divided into the four steps listed in Table 4. The majority of NMC will be detected at low rotational speed in the beginning, while the majority of CB will be detected later at maximum speed. Short time intervals for the measurements of the transmission profiles were set right after increasing the speed. This avoids unsteady PSD due to particles sinking unnoticed.

Table 4
Standard operation procedure used for the particle size distribution measurement of lithium-ion battery recycling suspensions with a LUMiSizer analytical centrifuge.

Step	time/s	interval/s	profiles/–	speed/s^{-1}
1.	1200	4	300	200
2.	300	2	150	2000
3.	750	5	150	4000
4.	82,500	250	330	4000

After the triplicate measurement, PSDs based on the density of NMC or CB were exported from the software. An analysis applying different densities in different size ranges is not possible. The mixture of the NMC and CB produces a bimodal PSD. Its saddle point can be assumed as the crossover between the bigger NMC- and the smaller CB-particles. The exported PSDs were cut there, and the density of NMC was used for the particle size range above the saddle point, and the density of CB was used below. The recombination resulted in a proper density-revised PSD.

Elemental analysis using inductively coupled plasma optical emission spectroscopy (ICP-OES)

For the ICP-OES measurement, the samples had to be dissolved in acid to ensure a homogeneous distribution of all elements. Each sample (~2 g of recycling suspension including the solvent) was mixed with 5 mL subboilded nitric acid (HNO_3 65 % AnalaR Normapur, VWR, Germany), 1 mL hydrochloric acid (HCl 30 % Suprapur Supelco, Merck, Germany) and 5 mL ultrapure water (Ultra Clear (0.055 µS cm^{-1}), Evoqua, USA). The mixture was digested in a microwave oven at 230 °C for 25 min. After cooling, the samples were diluted to a final volume of 50 mL with ultrapure water. The element concentration in the digest was measured with an ICP-OES (iCap 7000, Thermo Fisher Scientific, USA), either in a radial or axial mode, depending on the expected concentration range. All samples were prediluted to minimize interferences and assure an optimal measurement range. A wide range of elements was analyzed and can be found in Table SI.5. The certified reference standard MISA 6 (LGC Standards, UK) was repeatedly measured to ensure precision and accuracy.

The samples of recycling suspension contain different amounts of NMC after the ultrasound treatment depending on the delamination degree. To enable a comparison of the aluminum impurities in the different samples, the mass fraction of aluminum in NMC ω_{Al} was calculated according to Eq. (4). The mass concentration of aluminum was divided by the sum of NMC and aluminum mass concentration. Oxygen is not detected in an ICP-OES and was considered proportionally in the equation. The ratio of the molar masses NMC including oxygen 97.2 g mol^{-1} and NMC excluding oxygen 65.2 g mol^{-1} extrapolates the missing mass of oxygen.

$$\omega_{Al} = \frac{\beta_{Al}}{\frac{97.2\,\mathrm{g\,mol^{-1}}}{65.2\,\mathrm{g\,mol^{-1}}} \cdot (\beta_{Li} + \beta_{Ni} + \beta_{Mn} + \beta_{Co}) + \beta_{Al}} \quad (4)$$

Crystallography analysis using X-ray diffractometry (XRD) coupled with rietveld refinement

In preparation for the XRD-analysis, the recycling suspension resulting from increasing solid content experiments (Section "Increasing solid content") were dripped onto a polypropylene foil for X-ray applications (Polypropylene Thin-Film 425 6.0 µm, Chemplex, USA) and dried overnight (≥16 h) at 60 °C. The foil was then mounted on a silicon mono-crystal for the measurement. Due to non-disclosure, solely the NMC by Gelon, which was used for the labCath, was crystallographically analyzed. This is indicated by purple color in Fig. 1.

To analyze the impact of the solvent alternatives on the crystal structure, 1 g of NMC powder was mixed with 10 mL of solvent in a 100 mL laboratory bottle and ultrasonicated for an extended time of 26 min at 80 °C. The suspension was filtered on a membrane (wwPTFE 0.45 µm 47 mm DISC, Pall, USA) afterwards and dried overnight (≥16 h) at 60 °C. The resulting powder was transferred to the sample cups.

Powder XRD analysis for bulk crystallography characterization of the NMC material was conducted using a AXS D8 with DAVINCI diffractometer (Bruker, Germany), utilizing the X-ray emission line of Cu-Kα1,2 with an average wavelength of 1.541 84 × 10^{-10} m, and operation voltage and current at 40 kV and 40 mA, respectively, for 1-D diffraction measurements. The 2θ scattering angular range was between 2° to 82°, measurement time of 0.6 s per step, and a 2θ angular increment of 0.02°. The instrument is coupled with a LYNXEYE XE-T detector (192-channel compound Si strip), with <380 eV energy resolution (for copper radiation energy). Qualitative or semi-quantitative characterization was performed with the Bruker EVA software.

The crystal structures were refined by using the computer software FullProf [64]. The Powder Diffraction File with collection code 166714 from the inorganic crystal structures database (ICSD) provided by the Leibniz Institute for Information Infrastructure (FIZ Karlsruhe) [65] was used as reference. The Rietveld refinement was performed with the parameters as set for the powder XRD measurement and a linearly interpolated background. The following parameters were refined: scale factor, zero-point displacement, unit cell parameters (a and c in R$\bar{3}$m space group), peak shape (Lorentzian), while in cases with platelet-like size effect, asymmetry, and preferred orientation (Spherical harmonics or March-Dollase coefficients). Instrument width and shape contribution was determined using the NIST SRM660 LaB_6 standard.

Workaround according to non-disclosure

On the one hand, the real industrial cathode production scrap originating from a gigafactory makes this study very up-to-date and highly relevant for companies and industrial partners. On the other hand, a compromise needs to be made on the level of detail of the published data, because some are classified confidential by the manufacturer. The experiments were carried out using indCath and labCath in parallel to complete the data and to keep up the scientific significance. First of all, the ultrasound parameters were studied and optimized on industrial rejects to proof the feasibility of the ultrasound delamination for them. This includes an optimization of delamination degree, PSD and aluminum impurities. The optimal parameters were then used to continue the experiments for both, industrial and laboratory cathodes. During the analytic part of the study, solely the restricted XRD was skipped for indCath and the results are published for labCath only (see purple elements in Fig. 1). It is likely that the industrially prepared material changes in a similar way because the parameters are not reduced anymore after optimization on the industrial material. However, the missing data for full certainty cannot be published at this time due to non-disclosure. All other analysis were conducted using the higher relevant indCath. Concerning the ICP-OES measurement, the baseline of impurity or doping elements in the pristine material was classified confidential too. Only differences are mentioned, which is fully sufficient to interpret the values as impurities from the recycling process.

Results and discussion

Delamination process parameters

The study of different ultrasound parameters is presented by Fig. 2. It shows that, at the latest after 15 min, each of the chosen frequencies 29 kHz, 40 kHz or 120 kHz closely reached complete delamination ($D \approx 1$). Regarding the frequency of 40 kHz, the plot nicely shows the increasing delamination degree with time. Starting from (60.1 ± 10.7) % after 5 min at 60 °C, it reached (100.4 ± 2.6) % after 15 min. This trend shows the dissolution of the binder in the solvent and the displacement of the particles by shear forces in the ultrasound field, taking a certain time, limiting the speed of delamination. A further raised temperature from 60 °C to 80 °C might increase the delamination, but the difference is statistically insignificant, as a two-sided t-test demonstrated. The values of single delamination experiments and the significance test are given in Table SI.1.

The delamination degree quickly reached (101.4 ± 0.6) % after 5 min at 60 °C, using the 29 kHz-resonator. This acceleration at first seems to be an improvement in comparison to 40 kHz, but high aluminum impurities massively reduce the value of the recycling product. Engineered NMC particles may contain Al_2O_3 as a surface coating in a range from

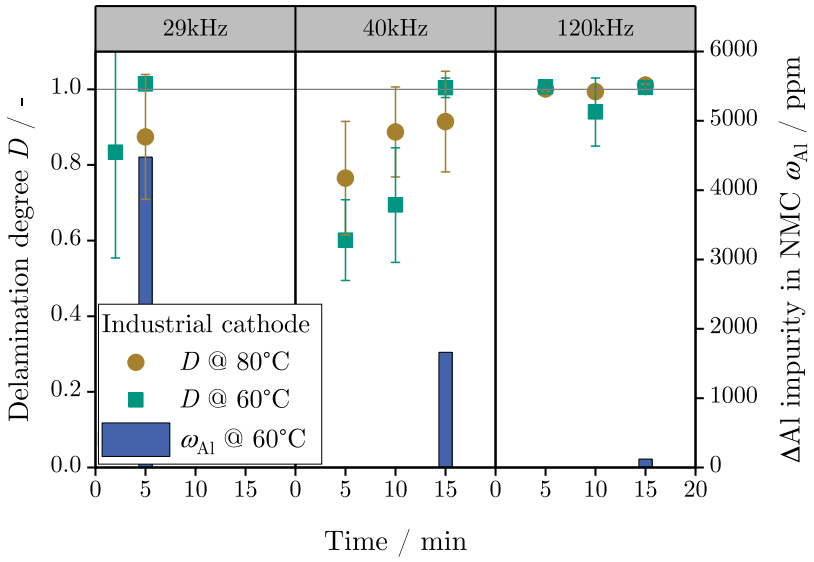

Fig. 2. Ultrasound induced delamination degree of lithium-nickel-manganese-cobalt-oxide (NMC) industrial cathodes (indCaths) in triethyl phosphate at varying temperature, time and frequency complemented by the aluminum (Al) impurities (Raw data given in Table SI.1 and Table SI.5.).

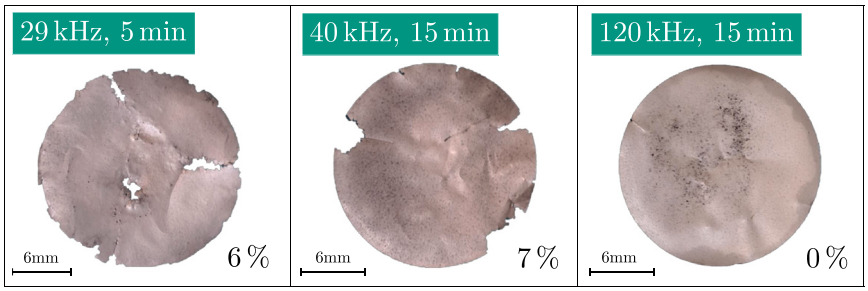

Fig. 3. Partial loss of area due to pitting of the current collector aluminum foil after ultrasound delamination with different frequencies at 60 °C.

several ppm to percent increasing the material's stability [66–68]. But the blue bars in Fig. 2 show a 4478 ppm higher aluminum content than in pristine NMC measured by ICP-OES. (The raw data is given in Table SI.5.) A critical level of 500 ppm metal impurities was independently mentioned as an industrial guideline for the reuse of recycled CAM by a battery-recycling company [69] and a battery-manufacturer. Reasons are mainly safety and liability concerns and not solely the lasting performance of the battery. This limit of additional impurities was exceeded by the delamination at 29 kHz after 5 min, and the material would not be reintroduced in the manufacturing process. The pitting, photographed in Fig. 3, was clearly identified as source of the massive aluminum impurities. It was estimated to 6 % of the current collector's area by image binarization. Due to closely complete delamination with simultaneously excessive aluminum impurities, the 29 kHz-experiment was prematurely aborted after 5 min as even higher impurities can be expected at longer residence times. In general, the mass loss of an aluminum plate also causes a defective calculation of the delamination degree, because the mass of aluminum is assumed constant in Eq. (2). This is the reason why D might occur slightly too high or can even reach > 1. The impact of pitting on the final delamination degree is negligible anyway, as the mass of the pitted aluminum is small among the whole electrode plate. For an exemplary calculation please refer to Appendix A. In addition, the parameter sets causing strong pitting disqualify themselves due to high impurities, not due to their delamination degree.

Regarding the 40 kHz-experiments, the impurity of 1661 ppm additional aluminum renders the material useless, as from the 29 kHz-experiments. The highest investigated frequency of 120 kHz combined quick and high delamination degree with little aluminum impurities. 120 kHz can meet the highly relevant criteria for industrial direct recycling and the reusability of the recycling product. (100.6 ± 0.1) % were reached after just 5 min at 60 °C. The pristine NMC's aluminum content was just exceeded by 121 ppm even after 15 min and a delamination degree of (100.5 ± 0.3) %. According to Šutilov et al. [60] and Neppiras et al. [70], the cavitation bubbles shrink with rising ultrasound frequency. At the same time, they occur in higher number concentration, but have less kinetic energy. This leads to little mechanical damage of the current collector during their collapse, barely causing aluminum contamination. This effect of gentler cleaning conditions at high frequencies is widely applied in megasonic cleaning of wafers [71, 72].

Further clarification on the high delamination degree can be derived from studies of ultrasound cleaning: Lower frequencies are used to mechanically remove microscopic contamination like particles (here: NMC and CB). High shear forces are generated by big collapsing cavitation bubbles and their micro jets, which pull off the contamination. High frequencies are applied to remove submicroscopic contamination. They are buried in the viscous boundary layer and are hardly subject to shear forces. High ultrasound frequencies diminish the boundary layer and cause a greater acoustic streaming in the solvent. This is heavily in favor of cleaning soluble contamination [73,74]. Transferred to the cathode delamination, high ultrasound frequencies likely support the dissolution of the binder, which might have led to high delamination degree even at high frequency. Both effects are probably present in all performed experiments, because the range of frequency does not exceed one magnitude. However, their part of contribution to the

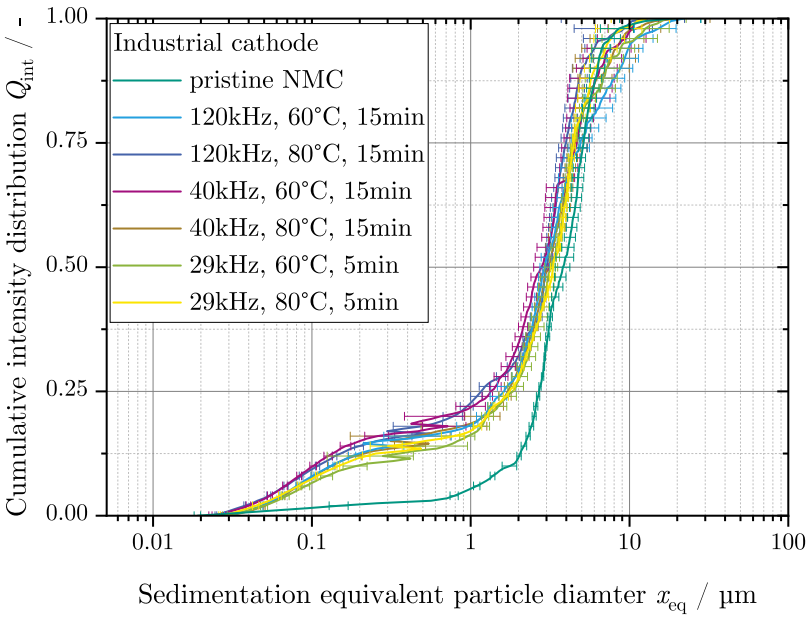

Fig. 4. Particle size distribution of regained recycling material containing lithium-nickel-manganese-cobalt-oxide (NMC) and carbon black after ultrasound treatment completed by the particle size distribution of pristine lithium-nickel-manganese-cobalt-oxide (characteristic values given in Table SI.2).

delamination process varies and affects the delamination result, as well as the contamination.

In order to assess the mechanical integrity of the CAM particles after the ultrasound treatment, the PSD is compared in Fig. 4. Pure and pristine NMC CAM serves as reference. Its PSD is represented by the light green graph. Continuing, the PSDs of the recycling suspensions originating from promising ultrasound parameter sets from Fig. 2 are plotted. They state that the PSD in the recycling suspension after ultrasound delamination was the same independently from frequency or temperature. Most eye catching difference to the pristine NMC is the rise in the particle size range from 0.02 µm to 0.5 µm. It can be explained by the CB additive in the cathode coating which is not included in the measurement of the pristine NMC. Solely comparing the NMC-correlated part (figuratively stretching the curves in direction of y-axis) no significant change in the particle size by the ultrasound treatment was observed. Very high sedimentation velocity of big and dense particles might have caused further little variations for particle sizes close to 10 µm. Anyway, the differences are very slight. The fact that the target NMC particles are not mechanically damaged during the ultrasound treatment, and primary particles can be regained, is very important for the applicability of this process (see Section "Particle size distribution (PSD)").

Solvent alternatives

According to the experiments with TEP, it is reasonable to chose the frequency of 120 kHz as the most appropriate one to further investigate different solvents for delamination. As rising the temperature had no negative effect while using TEP and might have positive effect on the dissolution by other solvents, the temperature was set to 80 °C. One goal of this experiment is to offer several different solvent alternatives and in comparison to identifying a suitable solvent, adapting the temperature in this range is facile. All solvent experiments were run at the same parameters (120 kHz, 80 °C), except from acetone whose temperature was limited to 50 °C due to its boiling point at ambient pressure. For high pressure experiments please refer to [75]. Fig. 5 shows the delamination degree in different green solvent alternatives. GVLA reached (100.1 ± 0.4) % within 15 min while cyrene, EAA and acetone did not exceed 31 %. TEP and DMSO completed the delamination earlier and so the experiments were stopped after 5 min. The different color of the diagram's bars intend to indicate the difference in delamination speed. These two solvents are therefore promising nominees to replace NMP in the direct recycling process. For comparison with the industrial standard solvent in LIB production, NMP delaminated (99.4 ± 0.6) %. Single experiment data on the delamination with solvent alternatives is given in Table SI.3.

It is remarkable that DMSO, being more distant in Hansen space, reaches better delamination than EAA. Higher distances than a non-solute would lead one to expect non-solubility in the first place. Studying the method of Hansen solubility sphere in depth reveals that it is an empirical correlation without any claim of absoluteness. It is also stated in [54,76] that especially smaller molecules promote little chemical resistance and thermodynamic encouragement, particularly better diffusion, penetration, and smaller free energy of mixing. They could unexpectedly dissolve a polymer better than predicted from the Hansen parameters. Hansen [54] therefore suggests to check potential outliers according to their molar volume. Comparing the molar volume of DMSO (71.1 $cm^3\ mol^{-1}$) and EAA (125.6 $cm^3\ mol^{-1}$) gives an indication that this might be the case here.

Another requirement to the solvents is that they are inert to NMC. They should not damage its crystal structure, which is relevant for the battery's electrochemical performance and investigated by XRD. The X-ray diffractogram of the pristine NMC cathode material in Fig. 6 shows well expressed diffraction peaks. The crystal structure corresponds to the rhombohedral $R\bar{3}m$ space group [77], without any characteristics pointing to the presence of a C2/m phase [78,79]. The refined diffractogram of the pristine NMC in Appendix C Fig. C.2 agrees with literature [80]. More specifically, it shows under-calculated intensity values primarily of the 00l peaks, e.g., 003 and 009, and secondarily of h0l peaks, e.g., 107. This feature is most probably attributed to the presence of crystallites stacked along *c*-axis direction. These have increased average diameter and express non-systematic inaccuracies in relative intensities [81] in comparison to the rest of the NMC crystallites. Milling of the material would show refined diffractograms similar to the ones in [82].

The diffraction peaks of the pristine NMC and the material subjected to ultrasonication with different solvents show both comparable and contrasting features. The 003 peak e.g. (see zoom in Fig. 6) is expressed between 18.69° and 18.74°. The higher 2θ refers to the pristine material (18.74°). Almost identical peak position, with an insignificant shift to

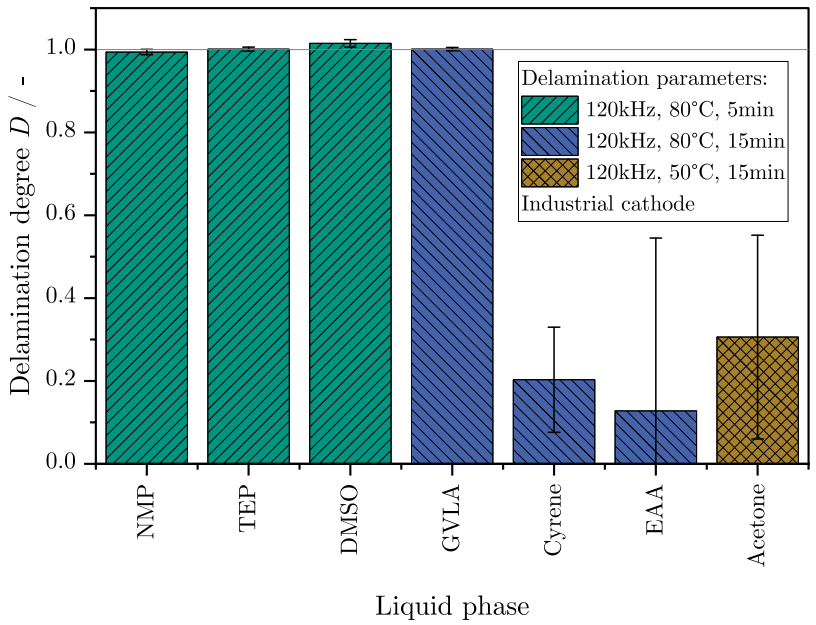

Fig. 5. Ultrasound induced delamination degree of industrial cathodes in different process liquids: N-methyl-2-pyrrolidone (NMP), triethyl phosphate (TEP), dimethyl sulfoxide (DMSO), γ-valerolactone (GVLA), cyrene, ethyl acetoacetate (EAA) and acetone (raw data is given in Table SI.3).

lower degrees, is observed for the ultrasonicated material, with the corresponding peaks to be located at 18.69° and 18.71°, for TEP and GVLA, respectively. The width of the 003 peak for these three samples is accordingly similar. Higher degree diffraction peaks (101, 006, 102, 104, etc.) exhibit exactly the same features.

The 0.05° 2θ shift of the 003 diffraction peak and analogous shifts for other peaks might be attributed to different processes. Firstly, minor potential intercalation of Ca^{2+}-cations from the TEP solvent in the layered structure of the NMC, could exhibit subordinate lattice distortions. On the other hand, minor intercalation of Mg^{2+}-cations from the GVLA solvent show much less crystal lattice distortion and near identical peak positions. The ionic radius of Mg^{2+} compared to Ca^{2+} is much more similar to Li^{+} with 2.44 % and 31.7 % relative difference in octahedral coordination, respectively [83]. This could result in the observed outcome. The changes in calcium and magnesium concentration measured by ICP-OES (Table 5) support this hypothesis. The result of reactions in the interface between Ca^{2+} or Mg^{2+} in the solvents and the NMC surface could be studied by high spatial resolution microanalytical techniques capable of achieving low detection limits, e.g., laser ablation-inductivly coupled plasma-mass spectroscopy (LA-ICP-MS) or focused ion beam-time of flight-secondary ion mass spectroscopy (FIB-ToF-SIMS). High spatial resolution techniques could reveal a radial gradient of these elements' concentration across the NMC particle cross-section.

Though the potential source of calcium or magnesium is proposed to be the solvent in each case, an intercalation mechanism for Ca^{2+} and Mg^{2+} in the NMC alkali layers is not well-understood yet. To our knowledge, research on Ca^{2+} and Mg^{2+} intercalation is primarily limited to (a) post-lithium batteries, i.e., Ca-ion and Mg-ion batteries and to cathode active materials which are not related to NMC [84–87], and (b) Ca^{2+} or Mg^{2+} doping in the transition metal layers of the NMC [88,89]. Additionally, diffraction peak shifts related to the 00l peaks could be also related to crystallographic expansion and, hence lattice strain due to solvent co-intercalation [90], although the phenomenon is best described in graphite [91,92], and layered sodium transition metal sulfides [93], which have received more attention. Prime candidates for solvent co-intercalation are materials characterized by quite weak interlayer binding energies [90], like layered materials distinguished by van der Waals interlayer forces, i.e. not NMC material.

Furthermore, small diffraction peak shifts could be attributed to the experimental conditions and, more specifically, to potential exposure

Table 5
Brief extract of relevant elements from the inductively coupled plasma optical emission spectroscopy measurements of the solvent alternatives triethyl phosphate (TEP), dimethyl sulfoxide (DMSO) and γ-valerolactone (GVLA) to compare calcium (Ca), magnesium (Mg) and Li content before and after ultrasonication and filtration with lithium-nickel-manganese-cobalt-oxide (NMC) (further elements are given in Table SI.5.).

Sample	Li/mg L^{-1}	Ca/mg L^{-1}	Mg/mg L^{-1}
Pristine TEP solvent	<0.003[a]	5.92	0.03
TEP+NMC-filtrate	7.23	<0.021[b]	0.08
Pristine DMSO solvent	<0.003[a]	2.87	0.02
DMSO+NMC-filtrate	25.03	<0.007[a]	<0.000[a]
Pristine GVLA solvent	0.11	<0.007[a]	0.01
GVLA+NMC-filtrate	3.37	<0.007[a]	0.00

[a] Limit of quantification
[b] limit of detection

to moisture or CO_2 from the atmosphere [94]. This is explained via a H^{+}/Li^{+} exchange mechanism [95] and further aging process and reaction with CO_2. Nonetheless, our XRD patterns show no lithium hydroxide or lithium carbonate formed in the experiment, processes and analysis timeframe [96–98] and even not after 6 weeks (see Appendix B). Thus, most probably the diffraction peak shifts are not connected to the storage of the NMC material.

Dissimilar to TEP and GVLA, the ultrasonicated material in the DMSO solvent show a more significant shift to lower 2θ degrees and, more importantly, double diffraction peaks or peak splitting. The (003) peak is expressed at 18.55° and 18.69° for the CAM in DMSO. The increased shift could correspond to a potentially stronger chemical process compatible with this feature. The hypothesis for intercalation of primarily Ca^{2+} and subordinately Mg^{2+} in the crystal lattice could stand, as well as the solvent co-intercalation, as discussed. Additionally, towards this direction, higher amount of lithium was leached from the NMC material by DMSO. However, the double peak feature might correspond to possibly a partial phase segregation [99,100], or be apparent and traced to inter-particle heterogeneity caused by electro-autocatalytic reactions in an NMC particle [101].

As a hypothesis, we investigate peak splitting that might be then attributed to the formation of two separate lithium-transition metal oxides, with fractionated contents of nickel, cobalt and/or manganese

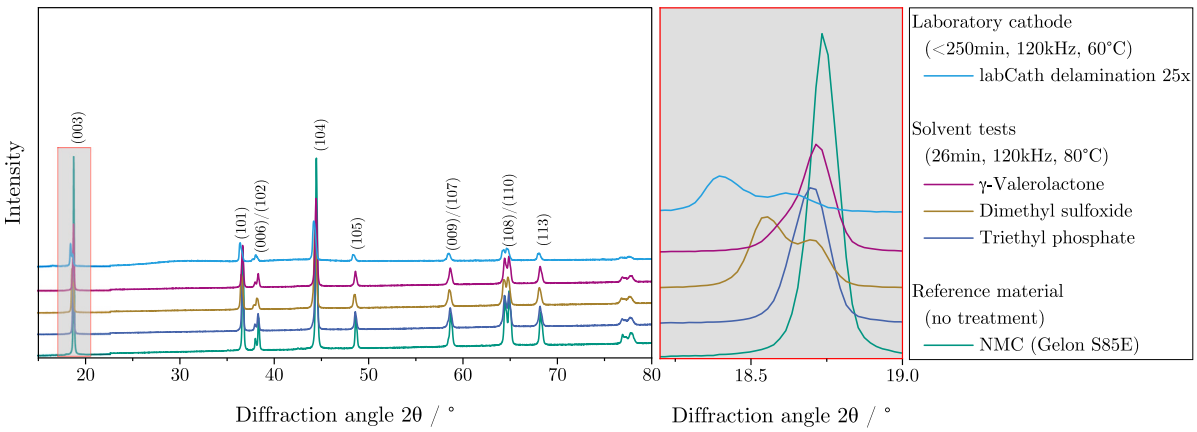

Fig. 6. X-ray diffractometry of lithium-nickel-manganese-cobalt-oxide (NMC) after ultrasound treatment at in different process liquids and solvents compared to pristine NMC and the diffractogram of regained NMC after increasing solid content experiments.

between them. The hypothesis is supported by the crystal refinement of the ultrasonicated material, with substitution of Li^+ in the lattice by Mg^{2+} and Ca^{2+}, by around 0.01 and 0.02 atoms per formula unit (apfu), respectively (Appendix C Table C.1 and Fig. C.4). In all cases, anti-site Li^+-Ni^{2+} substitution, as described in [102] as paired anti-site defects, seems more limited. The cases with suspected Li-loss agree with refined structures with shorter unit cell dimension along the *c*-axis. Additionally, relative to the pristine NMC, both average crystallite size and micro-strain show lower respective values.

A verification of the hypothesis on lattice distortion and phase segregation requires the use of transmission electron microscopy, possibly coupled with electron energy loss spectroscopy, and then better constrained further crystallographic refinement. A fractionation of nickel, manganese and cobalt and the degree of calcium and magnesium intercalation in the NMC layered structure could then be clearly identified.

Increasing solid content

To study the impact of increasing solid content, the best parameters from the previous experiments in Section "Delamination process parameters" were chosen. An ultrasound frequency of 120 kHz at a temperature of 60 °C delaminated the cathodes in TEP entirely. The residence time was set to 10 min to have some reserves when the solids hampers the delamination. The plot in Fig. 7 shows that the delamination can be repeated in the same bottle of solvent for multiple times. This was limited by a growing amount of sediment sticking to the plates when removing them from the bottle. It was therefore also necessary to rinse the plates in a separate beaker before drying them for the gravimetric determination of delamination efficiency.

The brown points originate from experiments using indCath. Despite some outliers, the delamination degree stays high until a solid content of 20 wt %. The used indCath were classified as production scrap and could include inhomogeneous mixing, defective coating or local compression [103] which might be a reason for the volatile delamination degree. As an average of all 25 repetitions, the delamination degree was (86.8 ± 19.3) % high and can be assumed to be in a suitable range for application. A dual-stage set-up could support the robustness of the process in future applications and would avoid problems by sediment adhesion.

The delamination of labCath can be repeated at least for 25 times too. The average delamination degree was (94.9 ± 9.1) % and never decreased below (76.2±36.9) % until a solid content of (15.90±0.38) wt %. Single experiment values are given in Table SI.4. In contrast to indCath, the labCath have not been calendered, which probably was the reason for the higher delamination degree. Another reason is that the labCath experiments did not reach as high solid contents as indCath due to one-sided manner of coating. Anyway, purpose of the parallel experiment with labCath was to investigate crystallographic changes of the material after the recycling process with subsequent XRDanalysis. Main focus in terms of delamination degree is on indCath.

The X-ray diffractogram of labCath material after 25 repetitions in TEP (see Fig. 6) shows distinct peak shift and splitting of the 003 peak. The changes are more pronounced than during the experiment with DMSO. It is significant that pristine NMC material did not change during 26 min of ultrasonication but did during the increasing solid content experiment. This may be due to the extremely extended experiment duration to up to 250 min, during which time the material is exposed to ultrasound and solvent. This issue will be reduced in future scale-up studies. High amounts of cathodes will be treated at the same time under exploiting a maximum of solid content and therefore much faster. Anyway, residence time needs to be considered as an important parameter. The storage of the material was under dry argon atmosphere (<10 ppm H_2O), while the experiments took place under ambient atmospheric conditions. This may also be a reason for structural changes [104], however, based on the previous discussion and time dependent XRD measurements of the pristine NMC as control material, it does not seem to be the case. In industrial applications, the recycling steps would take place under dry room conditions, hence, no issues are expected in this concern.

Outlook: Wet electrodes

When considering the entire variations of production scrap, not only dry rejects occur. Electrolyte-filled and formed cells are the most complex version of production scrap. As an outlook to recycle these as well, shipping returned cells were disassembled by hand and not further optimized ultrasound delamination experiments were performed on the cathodes. They are from the same type as the industrial ones described in Section "Raw materials". Fig. 8 shows that the ultrasound delamination degree is lower than for dry production scrap, and that the variation between the samples is higher. Wet scrap indCath got delaminated by (66.0 ± 16.9) % within 5 min, while dry scrap got delaminated completely. (77.5 ± 15.1) % of the coating's mass was removed after 15 min. The ultrasound delamination is also feasible with formed and electrolyte-wet cells, but might take longer exposure time or does not reach as high delamination degree as dry scrap in terminal state. Electrolyte in the porous electrode structure which needs to be displaced by the solvent before dissolving the binder can be a reason for that. Research on this hypothesis, as well as an optimization of the process parameters especially for wet scrap, will be conducted for further publication.

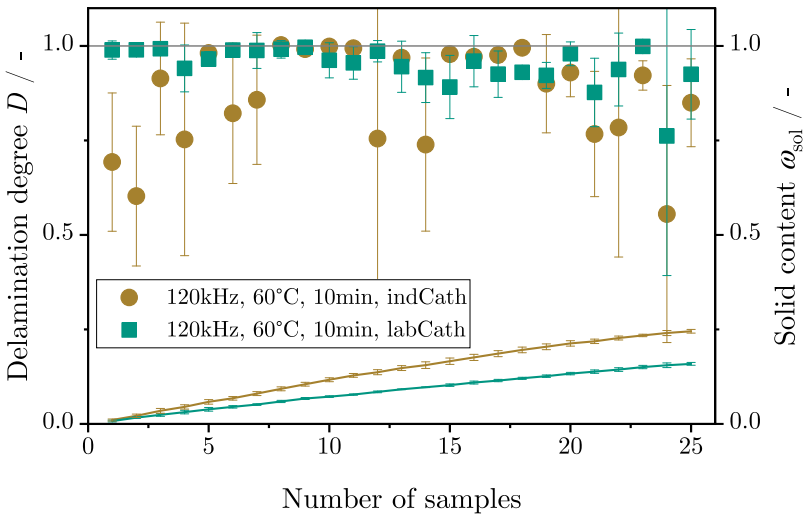

Fig. 7. Delamination degree of industrial and laboratory cathodes while increasing the solid content in the triethyl phosphate solvent by reapplying suspension for new sample plates further and further (raw data given in Table SI.4).

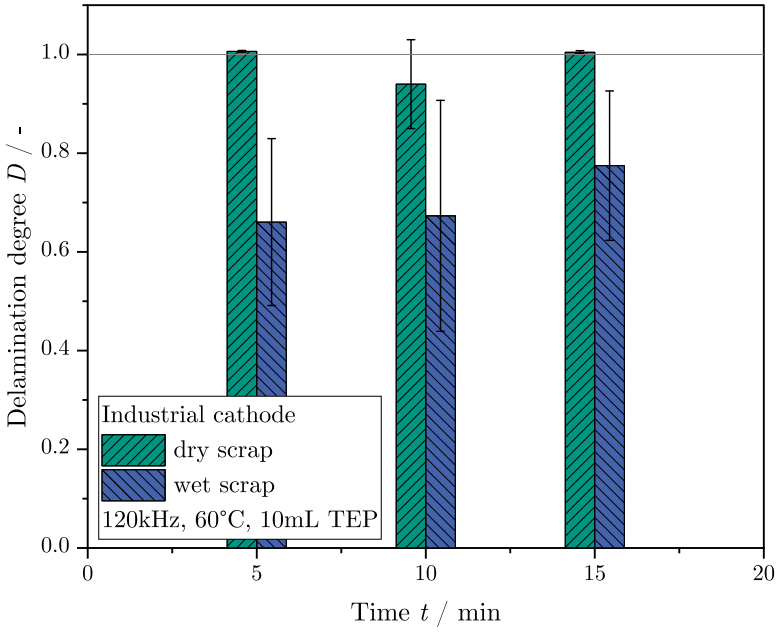

Fig. 8. Delamination degree of wet and dry production scrap in comparison after different time intervals.

Conclusions

Ultrasound has been considered as an effective process step for electrode delamination in direct battery recycling by several studies. This work gives further insights in delamination conditions by varying important process parameters. Central findings of this study are:

- *Solvent selection:* A suitable solvent needs to be chosen to successfully delaminate PVDF-binder based NMC-cathodes. The reproductive toxic, but in battery production commonly used solvent NMP could be replaced by less critical, green alternatives. Most promising candidate is TEP, which reached a comparable high delamination degree and little structural changes of the active material. It is therefore possible to fulfill the thought of sustainability in recycling even more when considering solvent alternatives in a conceptualization of a battery recycling plant. Anyway, there can be reasons to stick with NMP e.g. the integration of an in-house production scrap recycling in an existing production line. It is reasonable to assume that the results using TEP in this study can be reached or even exceeded by NMP due to its better PVDF-solubility.
- *Process temperature:* Elevated temperatures were necessary to basically enable the binder dissolution, but no significant effect between 60 °C and 80 °C on the delamination degree was observed.
- *Ultrasound frequency:* The ultrasound frequency played a crucial role in terms of delamination speed and purity of the recyclate. It turned out that only the application of high frequencies, like 120 kHz, can meet the purity requirements for recycling-NMC. Contrary, lower frequencies corroded the current collector quickly and caused high aluminum impurities. This study recommends to apply high ultrasound frequencies to avoid undesirable impurities. Mechanical damage of the monocrystalline NMC-particles seemed not to be an issue, as the PSD did not change during all of the experiments.

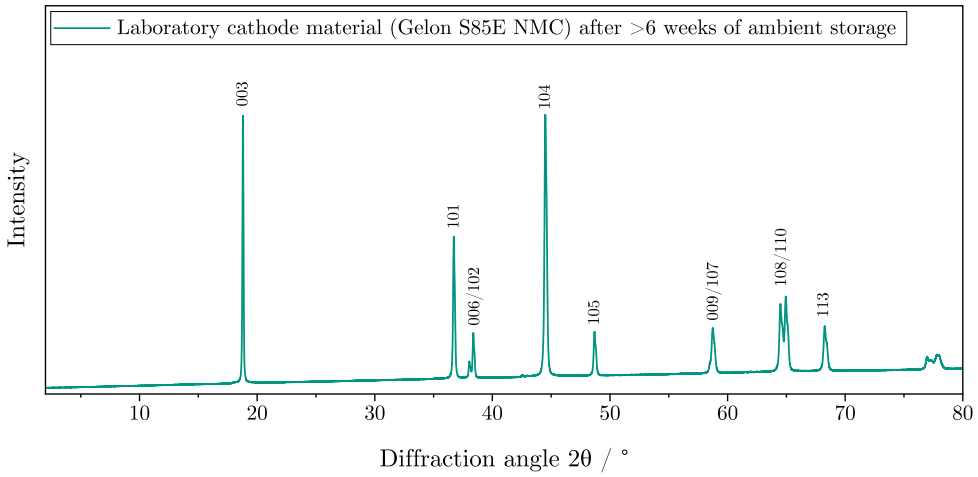

Fig. B.1. X-ray diffractometry of lithium-nickel-manganese-cobalt-oxide (NMC) used in the laboratory cathode (Gelon S85E) after an ambient storage time of minimum 6 weeks not indicating the formation of lithium hydroxide or lithium carbonate.

- *Solid content:* The increasing solid content experiments showed high delamination degree until $\geq 20\,\%$ and laid the foundation for a scale-up.

The development of a direct recycling process can be guided by the findings of this study. It opens up important design parameters which strongly influence the success of ultrasound delamination and the reusability of the recycling product. It is therefore suggested to pursue from the following:

- *Scale-up:* For sure, the development of a scalable process on technical scale needs to be done in future. This maximizes the yield of recyclate and minimizes the solvent consumption at the same time.
- *Pre-thickening:* A pre-thickening of the suspension during the delamination step can facilitate the further processing to a slurry for production of new batteries [34].
- *Cell tests:* The preceding points result in higher amounts of recyclate. This enables the preparation of sample cells to further characterize the electro-chemical integrity of the material, which will be part of following studies in this project.

CRediT authorship contribution statement

Steffen Kaiser: Writing – review & editing, Writing – original draft, Visualization, Validation, Supervision, Resources, Project administration, Methodology, Investigation, Formal analysis, Data curation, Conceptualization. **Christian Geier:** Methodology, Investigation, Formal analysis, Data curation. **Alexander Kessler:** Methodology, Investigation, Formal analysis, Data curation. **Christoforos Zamparas:** Writing – review & editing, Writing – original draft, Validation, Methodology, Investigation, Formal analysis, Data curation. **Elisabeth Eiche:** Writing – review & editing, Writing – original draft, Supervision, Resources, Project administration, Methodology, Investigation, Funding acquisition, Formal analysis, Data curation. **Marco Gleiß:** Writing – review & editing, Supervision, Resources, Project administration, Funding acquisition, Formal analysis, Data curation.

Declaration of competing interest

The authors declare that they have no known competing financial interests or personal relationships that could have appeared to influence the work reported in this paper.

Acknowledgments

The project DiRecReg on which this publication is based was funded by the German Federal Ministry of Education and Research within the SynBatt funding program under the grant number 03XP0553C. The authors are responsible for the contents of this publication. We thank Thomas Dreyer of the Weber Ultrasonics AG for the supply of the ultrasound device, the cavitation noise level measurements and the excellent collaboration in this project.

Appendix A. Error by pitting

Pitting makes $\leq 7\,\%$ of the current collector's area and the current collector itself is averagely $10.1\,\%$ of the electrode only. The error in the delamination degree is therefore below a one digit percentage and negligible for a comparison of the process parameters. The effect is presented based on an artificial $100\,\%$-case with average values.

$$\bar{m}_{plate} = 161.7\,\text{mg}$$
$$m_{Al} = 16.5\,\text{mg}$$
$$m_{decoat} = 16.5\,\text{mg}$$

$$D = \frac{\bar{m}_{plate} - (m_{decoat} - 7\,\%)}{\bar{m}_{plate} - m_{Al}} = \frac{162.5\,\text{mg} - (16.5\,\text{mg}\ (-1.2\,\text{mg}))}{162.5\,\text{mg} - 16.5\,\text{mg}}$$
$$= 1.0000\ (+0.008)$$

Appendix B. Ambient storage of lithium-nickel-manganese-cobalt-oxide

See Fig. B.1 for the X-ray diffractogram.

Appendix C. Rietveld refinement

Find the visualized Rietveld refinement in Figs. C.2–C.7 and the corresponding data in Table C.1.

Appendix D. Supplementary data

Supplementary material related to this article can be found online at https://doi.org/10.1016/j.fub.2026.100176.

Data availability

The authors do not have permission to share data.

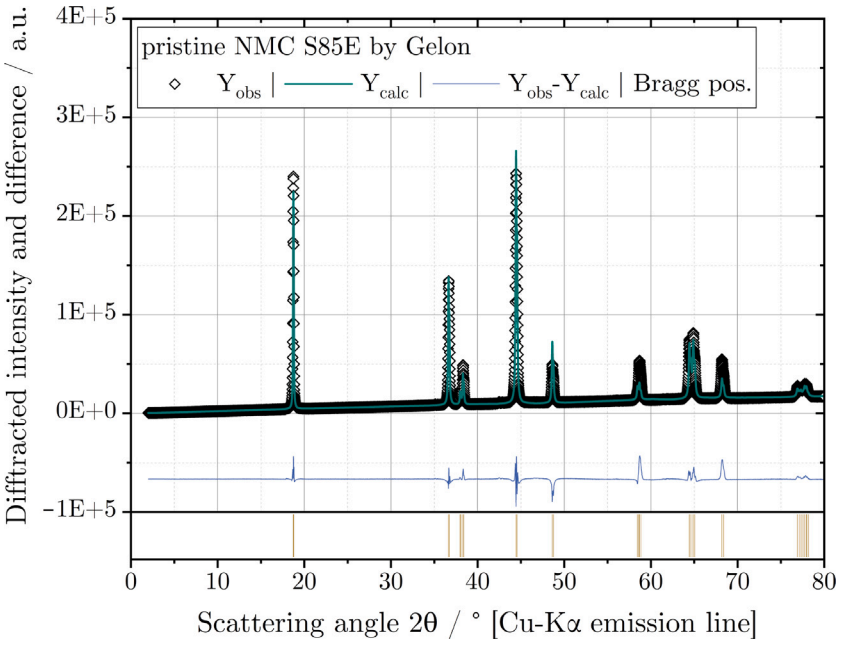

Fig. C.2. Rietveld refinement of pristine NMC crystal structure without ultrasonic treatment.

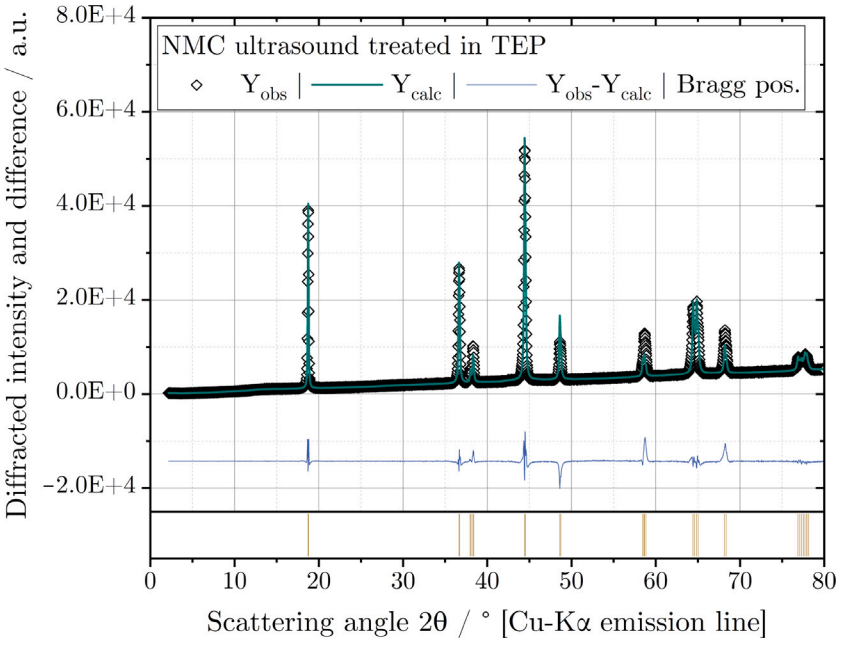

Fig. C.3. Rietveld refinement of NMC crystal structure after ultrasonic treatment in TEP (26 min, 120 kHz, 80 °C).

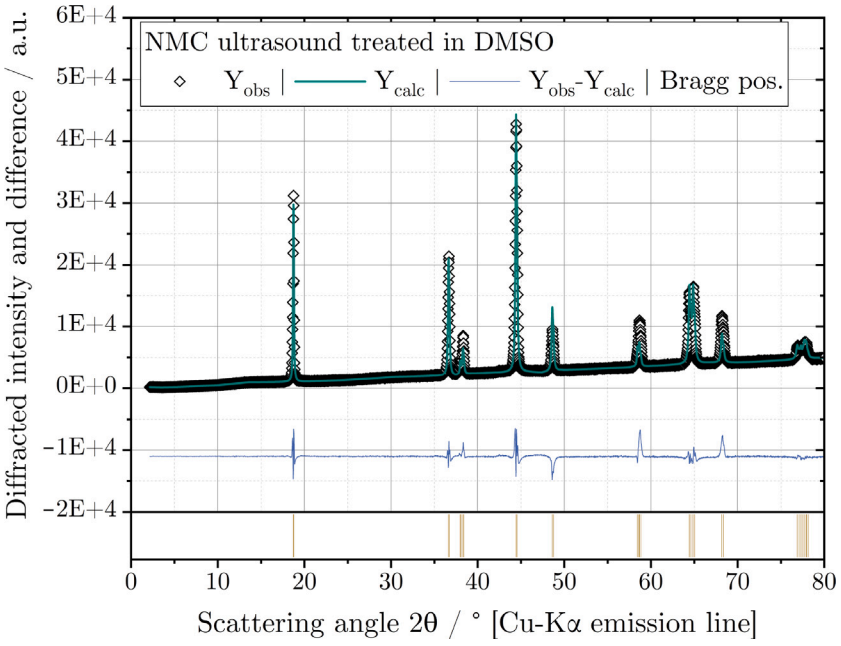

Fig. C.4. Rietveld refinement of NMC crystal structure after ultrasonic treatment in DMSO (26 min, 120 kHz, 80 °C).

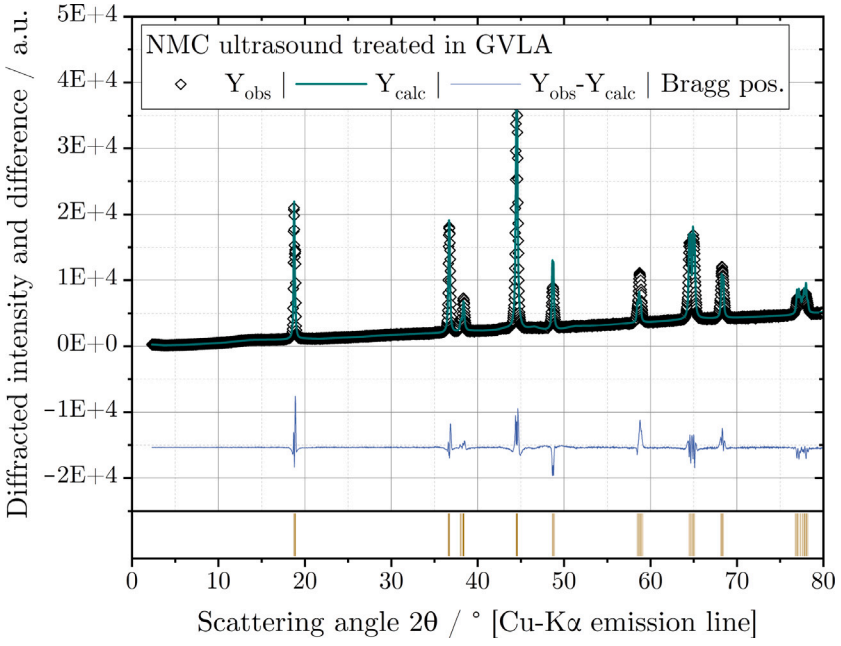

Fig. C.5. Rietveld refinement of NMC crystal structure after ultrasonic treatment in GVLA (26 min, 120 kHz, 80 °C).

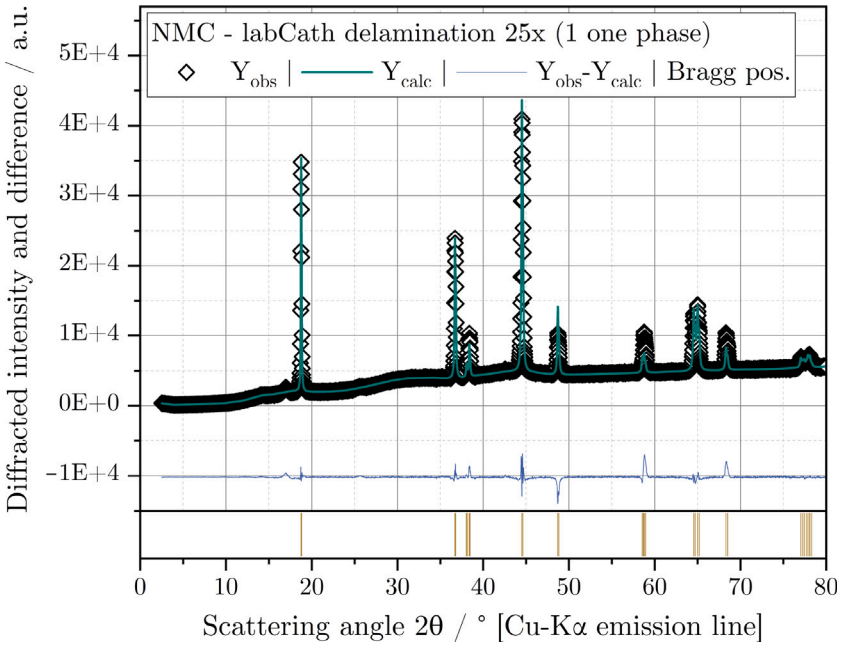

Fig. C.6. Rietveld refinement of NMC crystal structure after ultrasonic treatment in TEP during the increasing solid content delamination experiments (<250 min, 120 kHz, 60 °C).

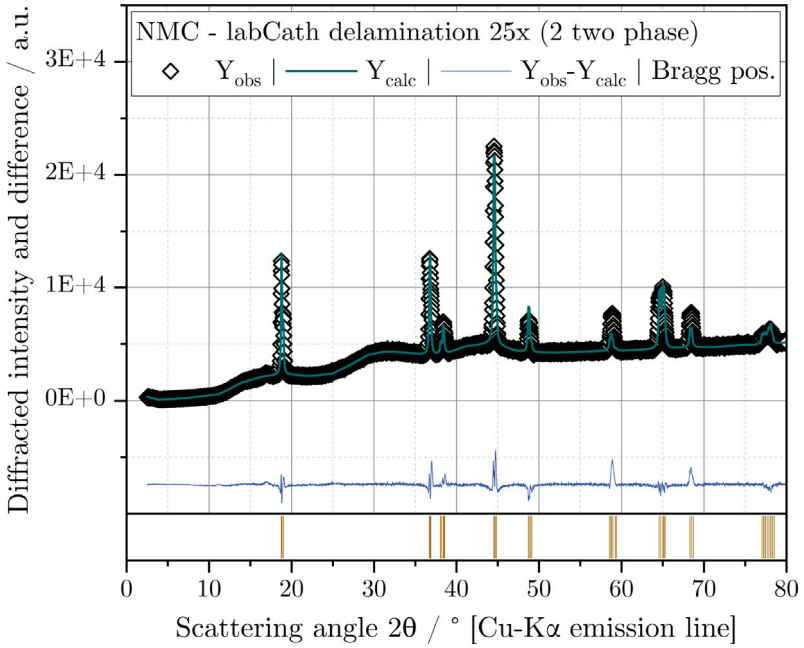

Fig. C.7. Rietveld refinement of NMC crystal structure after ultrasonic treatment in TEP during the increasing solid content delamination experiments (<250 min, 120 kHz, 60 °C).

Table C.1
Rietveld refinement of NMC crystal structure after ultrasonic treatment in different solvents and after the increasing solid content delamination experiment.

Refined structure (nominal NMC811)	Reliability factor	a (=b) /Å	c /Å	antisite Ni /apfu	Mg-in-Li /apfu	Ca-in-Li /apfu	Lithiation status	Average size /µm	St.d. size /µm	Av. micro-strain /%	St.d. micro-strain /%
pristine NMC (Gelon S85E)	2.01	2.871639	14.198465	0.043	n/a	n/a	normal	2.46	0.98	10.9	<0.01
NMC in TEP	3.51	2.872273	14.200033	0.005	0.011	0.022	normal	0.21	0.07	9.85	<0.01
NMC in GVLA	8.10	2.861912	14.022989	n/a	n/a	n/a	under	0.06	<0.01	n/a	n/a
		2.867333	14.175024	n/a	n/a	n/a	over	0.09	<0.01	6.03	<0.01
NMC in DMSO	5.01	2.872365	14.198237	0.025	0.001	0.010	normal	0.10	0.03	5.80	<0.01
labCath delamination 25x	4.91	2.867376	14.178411	0.036	n/a	n/a	normal	0.87	0.13	11.1	<0.01
	7.03	2.861912	14.022989	n/a	n/a	n/a	under	0.06	<0.01	n/a	n/a
		2.867333	14.175024	n/a	n/a	n/a	over	0.09	<0.01	6.02	<0.01

References

[1] S. Carrara, S. Bobba, D. Blagoeva, D.P. Alves, A. Cavalli, K. Georgitzikis, M. Grohol, A. Itul, T. Kuzov, C. Latunussa, L. Lyons, G. Malano, T. Maury, A.A. Prior, J. Somers, T. Telsnig, C. Veeh, D. Wittmer, C. Black, D. Pennington, M. Christou, JRC Publ. Repository (2023) http://dx.doi.org/10.2760/386650, URL https://publications.jrc.ec.europa.eu/repository/handle/JRC132889. (Accessed date 2025-01-20).

[2] B.E. Murdock, K.E. Toghill, N. Tapia-Ruiz, Adv. Energy Mater. 11 (39) (2021) 2102028, http://dx.doi.org/10.1002/aenm.202102028, URL https://onlinelibrary.wiley.com/doi/abs/10.1002/aenm.202102028. (Accessed date 2025-01-20).

[3] M.C. McManus, Appl. Energy 93 (2012) 288–295, http://dx.doi.org/10.1016/j.apenergy.2011.12.062, URL https://www.sciencedirect.com/science/article/pii/S0306261911008580. (Accessed date 2025-01-20).

[4] M. Chen, X. Ma, B. Chen, R. Arsenault, P. Karlson, N. Simon, Y. Wang, Joule 3 (11) (2019) 2622–2646, http://dx.doi.org/10.1016/j.joule.2019.09.014, URL https://linkinghub.elsevier.com/retrieve/pii/S254243511930474X. (Accessed date 2024-04-26).

[5] J. Fleischmann, M. Hanicke, E. Horetsky, D. Ibrahim, S. Jautelat, M. Linder, P. Schaufuss, L. Torscht, A. van de Rijt, McKinsey Company (2023).

[6] tagesschau.de, Baden-Württemberg: Batterien von E-Autos recyceln: Mercedes eröffnet seine erste Fabrik in BW. URL https://www.tagesschau.de/inland/regional/badenwuerttemberg/swr-kuppenheim-mercedes-benz-eroeffnet-seine-erste-batterie-recyclingfabrik-100.html. (Accessed date 2024-11-20).

[7] Duesenfeld, Duesenfeld: Umweltfreundliches Recycling von Lithium-Ionen-Batterien. URL https://www.duesenfeld.com/index_de.html. (Accessed date 2025-01-20).

[8] Li-Cycle, Li-Cycle: Lithium-ion Battery Recycling. URL https://li-cycle.com/. (Accessed date 2025-01-21).

[9] Primobius, Primobius: Batterie-Recycling ohne Grenzen. URL https://www.primobius.com/de-de. (Accessed date 2024-11-20).

[10] Umicore, Umicore Battery Recycling, 2023, URL https://www.umicore.com/en/newsroom/umicore-battery-recycling/. (Accessed date 2025-01-20).

[11] Z.J. Baum, R.E. Bird, X. Yu, J. Ma, ACS Energy Lett. 7 (2) (2022) 712–719, http://dx.doi.org/10.1021/acsenergylett.1c02602. (Accessed date 2024-11-11).

[12] G. Harper, R. Sommerville, E. Kendrick, L. Driscoll, P. Slater, R. Stolkin, A. Walton, P. Christensen, O. Heidrich, S. Lambert, A. Abbott, K. Ryder, L. Gaines, P. Anderson, Nature 575 (7781) (2019) 75–86, http://dx.doi.org/10.1038/s41586-019-1682-5, URL https://www.nature.com/articles/s41586-019-1682-5. (Accessed date 2023-11-09).

[13] M. Kaya, Circular Econ. 1 (2) (2022) 100015, http://dx.doi.org/10.1016/j.cec.2022.100015, URL https://www.sciencedirect.com/science/article/pii/S2773167722000152. (Accessed date 2025-01-21).

[14] C. Hanisch, J.-H. Schünemann, J. Diekmann, B. Westphal, T. Loellhoeffel, P.F. Przwiara, W. Haselrieder, A. Kwade, ECS Trans. 64 (22) (2015) 131, http://dx.doi.org/10.1149/06422.0131ecst, URL https://iopscience.iop.org/article/10.1149/06422.0131ecst/meta. (Accessed date 2023-11-06).

[15] S. Passerini, D. Bresser, A. Moretti, A. Varzi (Eds.), Encyclopedia of Electrochemistry, Wiley-VCH Verlag GmbH & Co. KGaA, Weinheim, Germany, 2020, http://dx.doi.org/10.1002/9783527610426.

[16] L. Yu, Y. Bai, B. Polzin, I. Belharouak, J. Power Sources 593 (2024) 233955, http://dx.doi.org/10.1016/j.jpowsour.2023.233955, URL https://www.sciencedirect.com/science/article/pii/S0378775323013319. (Accessed date 2025-01-22).

[17] J. Wu, M. Zheng, T. Liu, Y. Wang, Y. Liu, J. Nai, L. Zhang, S. Zhang, X. Tao, Energy Storage Mater. 54 (2023) 120–134, http://dx.doi.org/10.1016/j.ensm.2022.09.029, URL https://www.sciencedirect.com/science/article/pii/S2405829722005153. (Accessed date 2024-10-04).

[18] Y. Bai, N. Muralidharan, Y.-K. Sun, S. Passerini, M. Stanley Whittingham, I. Belharouak, Mater. Today 41 (2020) 304–315, http://dx.doi.org/10.1016/j.mattod.2020.09.001, URL https://www.sciencedirect.com/science/article/pii/S1369702120303060. (Accessed date 2024-06-18).

[19] A. Kwade, J. Diekmann (Eds.), Sustainable Production, Life Cycle Engineering and Management, Springer International Publishing, Cham, 2018, http://dx.doi.org/10.1007/978-3-319-70572-9, URL http://link.springer.com/10.1007/978-3-319-70572-9. (Accessed date 2023-11-20).

[20] J. Wang, J. Ma, Z. Zhuang, Z. Liang, K. Jia, G. Ji, G. Zhou, H.-M. Cheng, Chem. Rev. 124 (5) (2024) 2839–2887, http://dx.doi.org/10.1021/acs.chemrev.3c00884, URL https://doi.org/10.1021/acs.chemrev.3c00884. (Accessed date 2025-01-22).

[21] Y. Ji, E.E. Kpodzro, C.T. Jafvert, F. Zhao, Y. Ji, E.E. Kpodzro, C.T. Jafvert, F. Zhao, Clean Technol. Recycl. 1 (ctr-01-02-007) (2021) 124–151, http://dx.doi.org/10.3934/ctr.2021007, URL http://www.aimspress.com/rticle/doi/10.3934/ctr.2021007. (Accessed date 2023-11-07).

[22] D. Thompson, C. Hyde, J.M. Hartley, A.P. Abbott, P.A. Anderson, G.D.J. Harper, Resources, Conserv. Recycl. 175 (2021) 105741, http://dx.doi.org/10.1016/j.resconrec.2021.105741, URL https://www.sciencedirect.com/science/article/pii/S0921344921003505. (Accessed date 2025-01-24).

[23] S. Krüger, C. Hanisch, A. Kwade, M. Winter, S. Nowak, J. Electroanal. Chem. 726 (2014) 91–96, http://dx.doi.org/10.1016/j.jelechem.2014.05.017, URL https://www.sciencedirect.com/science/article/pii/S1572665714002033. (Accessed date 2025-01-23).

[24] N. Christian, J. Röder, S. Amrhein, A. Flegler, G. Giffin, Dry Delamination of LFP Cathodes via Induction Heating for Direct Recycling: A Novel Approach, 2024.

[25] C. Hanisch, T. Loellhoeffel, J. Diekmann, K.J. Markley, W. Haselrieder, A. Kwade, J. Clean. Prod. 108 (2015) 301–311, http://dx.doi.org/10.1016/j.jclepro.2015.08.026, URL https://www.sciencedirect.com/science/article/pii/S0959652615011154. (Accessed date 2025-01-22).

[26] W. Li, S. Yang, N. Liu, Y. Chen, Y. Xi, S. Li, Y. Jie, F. Hu, in: G. Gaustad, C. Fleuriault, M. Gökelma, J.A. Howarter, R. Kirchain, K. Ma, C. Meskers, N.R. Neelameggham, E. Olivetti, A.C. Powell, F. Tesfaye, D. Verhulst, M. Zhang (Eds.), REWAS 2019, Springer International Publishing, Cham, 2019, pp. 421–435, http://dx.doi.org/10.1007/978-3-030-10386-6_49.

[27] M. Wagner, D. Grießl, M. Hiller, A. Kwade, J. Clean. Prod. 428 (2023) 139338, http://dx.doi.org/10.1016/j.jclepro.2023.139338, URL https://www.sciencedirect.com/science/article/pii/S0959652623034960. (Accessed date 2025-01-24).

[28] S.L. Guzmán, M. Fehse, E. Gucciardi, M. Cabello, S. Martin, N. Etxebarria, M. Ceja, M. Romera, M. Galceran, M. Reynaud, J. Mater. Chem. A 13 (4) (2025) 2690–2706, http://dx.doi.org/10.1039/D4TA07642G, URL https://pubs.rsc.org/en/content/articlelanding/2025/ta/d4ta07642g. (Accessed date 2026-01-14).

[29] P. Li, S. Luo, G. Hao, K. Sun, Q. Liu, M. Møller, D. Wang, P.K.r. Kristensen, L. Gurevich, L.R. Jensen, L. Wang, X. He, J. Hazardous Mater. 481 (2025) 136553, http://dx.doi.org/10.1016/j.jhazmat.2024.136553, URL https://www.sciencedirect.com/science/article/pii/S0304389424031327. (Accessed date 2026-03-16).

[30] P. Li, S. Luo, Y. Lin, J. Xiao, X. Xia, X. Liu, L. Wang, X. He, Chemical Society Reviews 53 (24) (2024) 11967–12013, http://dx.doi.org/10.1039/D4CS00362D, URL https://pubs.rsc.org/en/content/articlelanding/2024/cs/d4cs00362d. (Accessed date 2026-03-16).

[31] M. Ahuis, A. Aluzoun, M. Keppeler, S. Melzig, A. Kwade, J. Power Sources 593 (2024) 233995, http://dx.doi.org/10.1016/j.jpowsour.2023.233995, URL https://www.sciencedirect.com/science/article/pii/S037877532301371X. (Accessed date 2025-01-20).

[32] C. Hanisch, W. Haselrieder, A. Kwade, in: J. Hesselbach, C. Herrmann (Eds.), Glocalized Solutions for Sustainability in Manufacturing, Springer, Berlin, Heidelberg, 2011, pp. 85–89, http://dx.doi.org/10.1007/978-3-642-19692-8_15.

[33] F. Denk, P. Wiechers, L. Lödige, S. Schabel, M. Gleiß, P. Scharfer, W. Schabel, J. Fleischer, in: K. Dröder, T. Vietor (Eds.), Circularity Days 2024, Springer Fachmedien, Wiesbaden, 2025, pp. 3–16, http://dx.doi.org/10.1007/978-3-658-45889-8_1.

[34] P. Wiechers, A. Hermann, S. Koob, F. Glaum, M. Gleiß, Batteries 10 (7) (2024) 218, http://dx.doi.org/10.3390/batteries10070218, URL https://www.mdpi.com/2313-0105/10/7/218. (Accessed date 2024-11-13).

[35] C. Lei, I. Aldous, J. M. Hartley, D. L. Thompson, S. Scott, R. Hanson, P. A. Anderson, E. Kendrick, R. Sommerville, K. S. Ryder, A. P. Abbott, Green Chem. 23 (13) (2021) 4710–4715, http://dx.doi.org/10.1039/D1GC01623G, URL https://pubs.rsc.org/en/content/articlelanding/2021/gc/d1gc01623g. (Accessed date 2024-04-26).

[36] Z. Tong, X. Ren, M. Ni, X. Bu, L. Dong, Energy Fuels 37 (19) (2023) 14574–14588, http://dx.doi.org/10.1021/acs.energyfuels.3c02290, URL https://doi.org/10.1021/acs.energyfuels.3c02290. (Accessed date 2025-01-24).

[37] S. Lim, S. Kim, K.H. Ahn, S.J. Lee, J. Power Sources 299 (2015) 221–230, http://dx.doi.org/10.1016/j.jpowsour.2015.09.009, URL https://www.sciencedirect.com/science/article/pii/S0378775315302718. (Accessed date 2025-01-27).

[38] X. Ren, Z. Tong, Y. Dai, G. Ma, Z. Lv, X. Bu, M. Bilal, A.B. Vakylabad, A. Hassanzadeh, Separations 10 (4) (2023) 246, http://dx.doi.org/10.3390/separations10040246, URL https://www.mdpi.com/2297-8739/10/4/246. (Accessed date 2025-11-05).

[39] 1-Methyl-2-pyrrolidinone - Safety Data Sheet, 2024, URL https://www.sigmaaldrich.com/DE/en/sds/sial/328634?userType=undefined.

[40] J. Sherwood, T.J. Farmer, J.H. Clark, Chem 4 (9) (2018) 2010–2012, http://dx.doi.org/10.1016/j.chempr.2018.08.035, URL https://www.sciencedirect.com/science/article/pii/S2451929418303887. (Accessed date 2025-01-27).

[41] O. Buken, K. Mancini, A. Sarkar, RSC Advanc. 11 (44) (2021) 27356–27368, http://dx.doi.org/10.1039/D1RA04922D, URL https://pubs.rsc.org/en/content/articlelanding/2021/ra/d1ra04922d. (Accessed date 2024-11-20).

[42] Z. Fang, Q. Duan, Q. Peng, Z. Wei, L. Jiang, J. Sun, Q. Wang, Green Chem. 25 (4) (2023) 1546–1558, http://dx.doi.org/10.1039/D2GC04436F, URL https://pubs.rsc.org/en/content/articlelanding/2023/gc/d2gc04436f. (Accessed date 2024-10-10).

[43] F. Heim, F. Langer, A. Paulus, T. Kreher, P. Birke, J. Power Sources 558 (2023) 232546, http://dx.doi.org/10.1016/j.jpowsour.2022.232546, URL https://www.sciencedirect.com/science/article/pii/S0378775322015233. (Accessed date 2024-02-09).

[44] H. Zhou, B. Pei, Q. Fan, F. Xin, M.S. Whittingham, J. Electrochem. Soc. 168 (4) (2021) 040536, http://dx.doi.org/10.1149/1945-7111/abf87d. (Accessed date 2024-07-08).

[45] C. Chen, V. Reddy Tatagari, H. Lin, L. Shaw, J. Energy Chem. 78 (2023) 240–245, http://dx.doi.org/10.1016/j.jechem.2022.12.006, URL https://www.sciencedirect.com/science/article/pii/S2095495622006659. (Accessed date 2024-02-09).

[46] Y. Bai, R. Essehli, C.J. Jafta, K.M. Livingston, I. Belharouak, ACS Sustain. Chem. Eng. 9 (17) (2021) 6048–6055, http://dx.doi.org/10.1021/acssuschemeng.1c01293. (Accessed date 2025-01-22).

[47] R. Sliz, J. Valikangas, H. Silva Santos, P. Vilmi, L. Rieppo, T. Hu, U. Lassi, T. Fabritius, ACS Appl. Energy Mater. 5 (4) (2022) 4047–4058, http://dx.doi.org/10.1021/acsaem.1c02923. (Accessed date 2024-11-20).

[48] L.-P. He, S.-Y. Sun, X.-F. Song, J.-G. Yu, Waste Manage. 46 (2015) 523–528, http://dx.doi.org/10.1016/j.wasman.2015.08.035, URL https://www.sciencedirect.com/science/article/pii/S0956053X15301021. (Accessed date 2025-01-20).

[49] W. Yang, Z. Tong, X. Bu, L. Dong, S. Chehreh Chelgani, ACS Omega 10 (11) (2025) 11214–11224, http://dx.doi.org/10.1021/acsomega.4c10547. (Accessed date 2026-03-11).

[50] E. Trebeck, A. Grams, J. Talkenberger, S. Prakash, J.E. Grimmenstein, T. Krampitz, H. Lieberwirth, A. Valenas, Recycling 10 (5) (2025) http://dx.doi.org/10.3390/recycling10050189, URL https://www.mdpi.com/2313-4321/10/5/189. (Accessed date 2026-03-13).

[51] Y. Yamada, Y. Kondo, H. Kondo, Waste Manage. 204 (2025) 114969, http://dx.doi.org/10.1016/j.wasman.2025.114969, URL https://www.sciencedirect.com/science/article/pii/S0956053X25003800. (Accessed date 2026-01-14).

[52] S. Henschel, S. Buschulte, F. Kößler, J. Fleischer, 35th CIRP Design 2025, Procedia CIRP 136 (2025) 787–791, http://dx.doi.org/10.1016/j.procir.2025.08.134, URL https://www.sciencedirect.com/science/article/pii/S221282712500887X. (Accessed date 2025-12-01).

[53] L. Lödige, T. Heckmann, P. Scharfer, W. Schabel, Batteries 11 (12) (2025) 436, http://dx.doi.org/10.3390/batteries11120436, URL https://www.mdpi.com/2313-0105/11/12/436. (Accessed date 2026-01-02).

[54] C.M. Hansen, Hansen solubility parameters: A user's handbook / Charles M. Hansen, ISBN: 978-0-8493-7248-3, 2007, URL https://katalog.bibliothek.kit.edu/cgi-bin/koha/opac-detail.pl?biblionumber=1000695&query_desc=hansen%20solubility.

[55] V.R. Ravikumar, A. Schröder, S. Köhler, F.A. Çetinel, M. Schmitt, A. Kondrakov, F. Eberle, J.-O. Eichler-Haeske, D. Klein, B. Schmidt-Hansberg, ACS Appl. Energy Mater. 4 (1) (2021) 696–703, http://dx.doi.org/10.1021/acsaem.0c02575. (Accessed date 2023-12-11).

[56] M. Wang, X. Dong, I.C. Escobar, Y.-T. Cheng, ACS Sustain. Chem. Eng. 8 (30) (2020) 11046–11051, http://dx.doi.org/10.1021/acssuschemeng.0c02884. (Accessed date 2026-03-16).

[57] A. Bottino, G. Capannelli, S. Munari, A. Turturro, J. Polym. Sci. Part B: Polym. Phys. 26 (4) (1988) 785–794, http://dx.doi.org/10.1002/polb.1988.090260405, URL https://onlinelibrary.wiley.com/doi/abs/10.1002/polb.1988.090260405. (Accessed date 2025-03-03).

[58] GESTIS-Stoffdatenbank. URL https://gestis.dguv.de/. (Accessed date 2026-03-13).

[59] W. Ultrasonics, Weber Ultrasonics AG, 2025, URL https://www.weber-ultrasonics.com/. (Accessed date 2025-01-30).

[60] V.A. Šutilov, P. Hauptmann, V.A. Šutilov, V.A. Šutilov, Physik des Ultraschalls: Grundlagen, Springer, Wien [u.a.], 1984.

[61] M. Stieß, Springer-Lehrbuch, Springer, Berlin, Heidelberg, 2009, http://dx.doi.org/10.1007/978/3-540-32552-9, URL http://link.springer.com/10.1007/978%2F3-540-32552-9. (Accessed date 2026-03-11).

[62] D. Lerche, J. Dispers. Sci. Technol. 23 (5) (2002) 699–709, http://dx.doi.org/10.1081/DIS-120015373, URL https://doi.org/10.1081/DIS-120015373. (Accessed date 2025-03-06).

[63] T. Yildiz, P. Wiechers, H. Nirschl, M. Gleiß, Next Energy 2 (2024) 100082, http://dx.doi.org/10.1016/j.nxener.2023.100082, URL https://www.sciencedirect.com/science/article/pii/S2949821X23000819. (Accessed date 2025-03-06).

[64] O. Arcelus, J. Rodríguez-Carvajal, N.A. Katcho, M. Reynaud, A.P. Black, D. Chatzogiannakis, C. Frontera, J. Serrano-Sevillano, M. Ismail, J. Carrasco, F. Fauth, M.R. Palacin, M. Casas-Cabanas, J. Appl. Crystallogr. 57 (5) (2024) 1676–1690, http://dx.doi.org/10.1107/S1600576724006885, URL https://journals.iucr.org/j/issues/2024/05/00/iu5063/. (Accessed date 2026-02-02).

[65] J.D. Wilcox, E.E. Rodriguez, M.M. Doeff, J. Electrochem. Soc. 156 (12) (2009) A1011, http://dx.doi.org/10.1149/1.3237100, URL https://iopscience.iop.org/article/10.1149/1.3237100/meta. (Accessed date 2026-02-02).

[66] A. Javed, A. Makvandi, F. Demelash, E. Adhitama, B. Heidrich, M. Peterlechner, G. Wilde, M. Winter, M. Börner, Batteries Supercaps 7 (6) (2024) e202300580, http://dx.doi.org/10.1002/batt.202300580, URL https://onlinelibrary.wiley.com/doi/abs/10.1002/batt.202300580. (Accessed date 2025-09-11).

[67] R.L. B. Chen, F. N. Sayed, H. Banerjee, I. Temprano, J. Wan, A. J. Morris, C. P. Grey, Energy Environ. Sci. 18 (4) (2025) 1879–1900, http://dx.doi.org/10.1039/D4EE03444A, URL https://pubs.rsc.org/en/content/articlelanding/2025/ee/d4ee03444a. (Accessed date 2025-10-07).

[68] B. Han, B. Key, A.S. Lipton, J.T. Vaughey, B. Hughes, J. Trevey, F. Dogan, J. Electrochem. Soc. 166 (15) (2019) A3679, http://dx.doi.org/10.1149/2.0681915jes, URL https://iopscience.iop.org/article/10.1149/2.0681915jes/meta. (Accessed date 2025-10-07).

[69] T. Weischer, On | Direct scrap recycling and in-house recycling, 2024, URL https://www.on-hosokawa.com/recycling-systems.

[70] E.A. Neppiras, Phys. Rep. 61 (3) (1980) 159–251, http://dx.doi.org/10.1016/0370-1573(80)90115-5, URL https://www.sciencedirect.com/science/article/pii/0370157380901155. (Accessed date 2025-07-25).

[71] R. Nagarajan, S. Awad, K.R. Gopi, in: R. Kohli, K.L. Mittal (Eds.), Developments in Surface Contamination and Cleaning, William Andrew Publishing, Oxford, 2011, pp. 31–62, http://dx.doi.org/10.1016/B978-1-4377-7885-4.10002-8, URL https://www.sciencedirect.com/science/article/pii/B9781437778854100028. (Accessed date 2025-07-28).

[72] A.A. Busnaina, I.I. Kashkoush, G.W. Gale, J. Electrochem. Soc. 142 (8) (1995) 2812, http://dx.doi.org/10.1149/1.2050096, URL https://iopscience.iop.org/article/10.1149/1.2050096/meta. (Accessed date 2025-07-28).

[73] D. McQueen, Ultrasonics 24 (5) (1986) 273–280, http://dx.doi.org/10.1016/0041-624X(86)90105-8, URL https://linkinghub.elsevier.com/retrieve/pii/0041624X86901058. (Accessed date 2024-11-15).

[74] M.O. Lamminen, H.W. Walker, L.K. Weavers, J. Membr. Sci. 237 (1) (2004) 213–223, http://dx.doi.org/10.1016/j.memsci.2004.02.031, URL https://www.sciencedirect.com/science/article/pii/S0376738804001978. (Accessed date 2024-11-15).

[75] G. Jiang, D. Lee, D. Raimbault, P.A. Anderson, G.A. Leeke, Resources, Conserv. Recycl. 209 (2024) 107778, http://dx.doi.org/10.1016/j.resconrec.2024.107778, URL https://www.sciencedirect.com/science/article/pii/S0921344924003720. (Accessed date 2026-03-12).

[76] M.J. Louwerse, A. Maldonado, S. Rousseau, C. Moreau-Masselon, B. Roux, G. Rothenberg, ChemPhysChem 18 (21) (2017) 2999–3006, http://dx.doi.org/10.1002/cphc.201700408, URL https://onlinelibrary.wiley.com/doi/abs/10.1002/cphc.201700408. (Accessed date 2026-03-19).

[77] J. Li, R. Shunmugasundaram, R. Doig, J.R. Dahn, Chem. Mater. 28 (1) (2016) 162–171, http://dx.doi.org/10.1021/acs.chemmater.5b03500, URL https://doi.org/10.1021/acs.chemmater.5b03500. (Accessed date 2025-09-02).

[78] R. Shunmugasundaram, R.S. Arumugam, J.R. Dahn, J. Electrochem. Soc. 163 (7) (2016) A1394, http://dx.doi.org/10.1149/2.1221607jes, URL https://iopscience.iop.org/article/10.1149/2.1221607jes/meta. (Accessed date 2025-09-02).
[79] E.M. Erickson, F. Schipper, T.R. Penki, J.-Y. Shin, C. Erk, F.-F. Chesneau, B. Markovsky, D. Aurbach, J. Electrochem. Soc. 164 (1) (2017) A6341, http://dx.doi.org/10.1149/2.0461701jes, URL https://iopscience.iop.org/article/10.1149/2.0461701jes/meta. (Accessed date 2025-09-02).
[80] J.I. Preimesberger, C.K. Kirwa, E. Allen, N.S. Dutta, E. Wang, F. Dogan, P. Walker, Y. Bai, K.Z. Pupek, L. Stanley, T.L. Kinnibrugh, M. Nisbet, T.T. Fister, H. Luo, J.E. Coyle, Chem. Mater. 37 (23) (2025) 9406–9419, http://dx.doi.org/10.1021/acs.chemmater.5c01824. (Accessed date 2026-02-02).
[81] L.B. McCusker, R.B. Von Dreele, D.E. Cox, D. Louër, P. Scardi, J. Appl. Crystallogr. 32 (1) (1999) 36–50, http://dx.doi.org/10.1107/S0021889898009856. (Accessed date 2026-02-02).
[82] X. Zhang, W.J. Jiang, A. Mauger, Qilu, F. Gendron, C.M. Julien, J. Power Sources 195 (5) (2010) 1292–1301, http://dx.doi.org/10.1016/j.jpowsour.2009.09.029, URL https://www.sciencedirect.com/science/article/pii/S0378775309016231. (Accessed date 2026-02-02).
[83] E.J.W. Whittaker, R. Muntus, Geochim. Cosmochim. Acta 34 (9) (1970) 945–956, http://dx.doi.org/10.1016/0016-7037(70)90077-3, URL https://www.sciencedirect.com/science/article/pii/0016703770900773. (Accessed date 2025-09-02).
[84] H. Bu, H. Lee, D. Setiawan, S.-T. Hong, Chem. Phys. Rev. 3 (1) (2022) 011309, http://dx.doi.org/10.1063/5.0073087. (Accessed date 2026-03-17).
[85] S. Cui, Y. Wang, D. Zeng, Z. Lv, A. Wang, A. Du, Z. Li, G. Cui, Adv. Sci. 12 (44) (2025) e08050, http://dx.doi.org/10.1002/advs.202508050, URL https://onlinelibrary.wiley.com/doi/abs/10.1002/advs.202508050. (Accessed date 2026-03-17).
[86] S. Vincent, J.H. Chang, P. Canepa, J.M. García-Lastra, Chem. Mater. 35 (9) (2023) 3503–3512, http://dx.doi.org/10.1021/acs.chemmater.2c03784, URL https://doi.org/10.1021/acs.chemmater.2c03784. (Accessed date 2026-03-17).
[87] T. Wei, X. Cheng, J. Dong, Y. Zhang, J. Zhang, M. Liang, J. Li, T.-F. Yi, Chinese Chem. Lett. (2025) 112087, http://dx.doi.org/10.1016/j.cclet.2025.112087, URL https://www.sciencedirect.com/science/article/pii/S1001841725012641. (Accessed date 2026-03-17).
[88] A. Gomez-Martin, F. Reissig, L. Frankenstein, M. Heidbüchel, M. Winter, T. Placke, R. Schmuch, Adv. Energy Mater. 12 (8) (2022) 2103045, http://dx.doi.org/10.1002/aenm.202103045, URL https://onlinelibrary.wiley.com/doi/abs/10.1002/aenm.202103045. (Accessed date 2026-03-17).
[89] S. Kaewmala, N. Kamma, S. Buakeaw, W. Limphirat, J. Nash, S. Srilomsak, P. Limthongkul, N. Meethong, Sci. Rep. 13 (1) (2023) 4526, http://dx.doi.org/10.1038/s41598-023-31492-0, URL https://www.nature.com/articles/s41598-023-31492-0. (Accessed date 2026-03-17).
[90] G.A. Ferrero, G. Åvall, K. Janßen, Y. Son, Y. Kravets, Y. Sun, P. Adelhelm, Chem. Rev. 125 (6) (2025) 3401–3439, http://dx.doi.org/10.1021/acs.chemrev.4c00805, URL https://doi.org/10.1021/acs.chemrev.4c00805. (Accessed date 2026-03-17).
[91] L. Li, Z. Hu, S. Zhao, S.-L. Chou, Chem. Sci. 12 (46) (2021) 15206–15218, http://dx.doi.org/10.1039/D1SC04202E, URL https://pubs.rsc.org/en/content/articlelanding/2021/sc/d1sc04202e. (Accessed date 2026-03-17).
[92] L. Tao, D. Xia, P. Sittisomwong, H. Zhang, J. Lai, S. Hwang, T. Li, B. Ma, A. Hu, J. Min, D. Hou, S.R. Shah, K. Zhao, G. Yang, H. Zhou, L. Li, P. Bai, F. Shi, F. Lin, J. Am. Chem. Soc. 146 (24) (2024) 16764–16774, http://dx.doi.org/10.1021/jacs.4c04594. (Accessed date 2026-03-17).
[93] Y. Sun, G. Åvall, S.-H. Wu, G. A. Ferrero, A. Freytag, P.B. Groszewicz, H. Wang, K.A. Mazzio, M. Bianchini, V. Baran, S. Risse, P. Adelhelm, Nat. Mateer. 24 (9) (2025) 1441–1449, http://dx.doi.org/10.1038/s41563-025-02287-7, URL https://www.nature.com/articles/s41563-025-02287-7. (Accessed date 2026-03-17).
[94] R. Jung, R. Morasch, P. Karayaylali, K. Phillips, F. Maglia, C. Stinner, Y. Shao-Horn, H.A. Gasteiger, J. Electrochem. Soc. 165 (2) (2018) A132, http://dx.doi.org/10.1149/2.0401802jes, URL https://iopscience.iop.org/article/10.1149/2.0401802jes. (Accessed date 2026-03-17).
[95] I.A. Shkrob, J.A. Gilbert, P.J. Phillips, R. Klie, R.T. Haasch, J. Bareño, D.P. Abraham, J. Electrochem. Soc. 164 (7) (2017) A1489, http://dx.doi.org/10.1149/2.0861707jes, URL https://iopscience.iop.org/article/10.1149/2.0861707jes. (Accessed date 2026-03-17).
[96] C. Busà, M. Belekoukia, M.J. Loveridge, Electrochim. Acta 366 (2021) 137358, http://dx.doi.org/10.1016/j.electacta.2020.137358, URL https://www.sciencedirect.com/science/article/pii/S0013468620317515. (Accessed date 2026-03-17).
[97] T. Langner, T. Sieber, A. Rietig, V. Merk, L. Pfeifer, J. Acker, Sci. Rep. 13 (1) (2023) 5671, http://dx.doi.org/10.1038/s41598-023-32688-0, URL https://www.nature.com/articles/s41598-023-32688-0. (Accessed date 2026-03-17).
[98] M. Winkowska-Struzik, D.A. Buchberger, W. Uhrynowski, M. Struzik, A. Czerwinski, ACS Omega 9 (51) (2024) 50334–50348, http://dx.doi.org/10.1021/acsomega.4c06636, URL https://doi.org/10.1021/acsomega.4c06636. (Accessed date 2026-03-17).
[99] S. Pereira, M.R. Correia, E. Pereira, K.P. O'Donnell, E. Alves, A.D. Sequeira, N. Franco, Appl. Phys. Lett. 79 (10) (2001) 1432–1434, http://dx.doi.org/10.1063/1.1397276, URL https://doi.org/10.1063/1.1397276. (Accessed date 2025-09-02).
[100] S. Pereira, M.R. Correia, E. Pereira, K.P. O'Donnell, R.W. Martin, M.E. White, E. Alves, A.D. Sequeira, N. Franco, Mater. Sci. Eng.: B 93 (1) (2002) 163–167, http://dx.doi.org/10.1016/S0921-5107(02)00039-9, URL https://www.sciencedirect.com/science/article/pii/S0921510702000399. (Accessed date 2025-09-02).
[101] J. Park, H. Zhao, S.D. Kang, K. Lim, C.-C. Chen, Y.-S. Yu, R.D. Braatz, D.A. Shapiro, J. Hong, M.F. Toney, M.Z. Bazant, W.C. Chueh, Nature Mater. 20 (7) (2021) 991–999, http://dx.doi.org/10.1038/s41563-021-00936-1, URL https://www.nature.com/articles/s41563-021-00936-1. (Accessed date 2026-03-17).
[102] L. Yin, Z. Li, G.S. Mattei, J. Zheng, W. Zhao, F. Omenya, C. Fang, W. Li, J. Li, Q. Xie, E.M. Erickson, J.-G. Zhang, M.S. Whittingham, Y.S. Meng, A. Manthiram, P.G. Khalifah, Chem. Mater. 32 (3) (2020) 1002–1010, http://dx.doi.org/10.1021/acs.chemmater.9b03646. (Accessed date 2026-02-02).
[103] A. Schoo, R. Moschner, J. Hülsmann, A. Kwade, Batteries 9 (2) (2023) http://dx.doi.org/10.3390/batteries9020111, URL https://www.mdpi.com/2313-0105/9/2/111. (Accessed date 2026-03-16).
[104] C. Lv, Z. Li, X. Ren, K. Li, J. Ma, X. Duan, J. Mater. Chem. A 9 (7) (2021) 3995–4006, http://dx.doi.org/10.1039/D0TA10378K, URL https://pubs.rsc.org/en/content/articlelanding/2021/ta/d0ta10378k. (Accessed date 2023-12-11).